

AD-A100 386

KUHN (RICHARD E) NEWPORT NEWS VA
AN ENGINEERING METHOD FOR ESTIMATING THE LATERAL/DIRECTIONAL CH--ETC(U)
FEB 81 R E KUHN

F/G 20/4

N62269-80-C-0386

NL

UNCLASSIFIED

NADC-81031-60

[]
AC
A 100 386

END

DATE

FILED

7 8!

DTIC

LEVEL

12

REPORT NO. NADC-81031-60



AD A100386

AN ENGINEERING METHOD FOR ESTIMATING THE LATERAL/DIRECTIONAL
CHARACTERISTICS OF V/STOL CONFIGURATIONS IN TRANSITION

Richard E. Kuhn
V/STOL Consultant
111 Misteltoe Drive
Newport News, Virginia 23606

FEBRUARY 1981

FINAL REPORT

AIRTASK NO. A03V-32D/01B/7F41-400-00

DTIC
S ELECT
JUN 18 1981
C

APPROVED FOR PUBLIC RELEASE; DISTRIBUTION UNLIMITED

Prepared for
NAVAL AIR DEVELOPMENT CENTER
Warminster, Pennsylvania 18974

DTIC FILE COPY

81 6 18 018


NOTICES

REPORT NUMBERING SYSTEM - The numbering of technical project reports issued by the Naval Air Development Center is arranged for specific identification purposes. Each number consists of the Center acronym, the calendar year in which the number was assigned, the sequence number of the report within the specific calendar year, and the official 2-digit correspondence code of the Command Office or the Functional Directorate responsible for the report. For example: Report No. NADC-78015-20 indicates the fifteenth Center report for the year 1978, and prepared by the Systems Directorate. The numerical codes are as follows:

CODE	OFFICE OR DIRECTORATE
00	Commander, Naval Air Development Center
01	Technical Director, Naval Air Development Center
02	Comptroller
10	Directorate Command Projects
20	Systems Directorate
30	Sensors & Avionics Technology Directorate
40	Communication & Navigation Technology Directorate
50	Software Computer Directorate
60	Aircraft & Crew Systems Technology Directorate
70	Planning Assessment Resources
80	Engineering Support Group

PRODUCT ENDORSEMENT - The discussion or instructions concerning commercial products herein do not constitute an endorsement by the Government nor do they convey or imply the license or right to use such products.

APPROVED BY:


E. J. STURM
CAPT USN

DATE:

4/27/81

REPORT DOCUMENTATION PAGE		READ INSTRUCTIONS BEFORE COMPLETING FORM
1. REPORT NUMBER NADC 81031-60	2. GOVT ACCESSION NO. AD-A100 386	3. RECIPIENT'S CATALOG NUMBER
4. TITLE (and Subtitle) AN ENGINEERING METHOD FOR ESTIMATING THE LATERAL/DIRECTIONAL CHARACTERISTICS OF V/STOL CONFIGURATIONS IN TRANSITION		5. TYPE OF REPORT & PERIOD COVERED Final Technical Report.
7. AUTHOR(s) Richard E. Kuhn		6. PERFORMING ORG. REPORT NUMBER
9. PERFORMING ORGANIZATION NAME AND ADDRESS Richard E. Kuhn, V/STOL Consultant 111 Mistletoe Drive Newport News, Virginia 23606		8. CONTRACT OR GRANT NUMBER(s) N62269-80-C-0366
11. CONTROLLING OFFICE NAME AND ADDRESS Naval Air Development Center Warminster, Pennsylvania 18974		10. PROGRAM ELEMENT, PROJECT, TASK AREA & WORK UNIT NUMBERS AIRTASK No. A03V-320D/ 01B/7F41-400-00
14. MONITORING AGENCY NAME & ADDRESS (if different from Controlling Office) 10 F 41-400-00 17 211 100-00		12. REPORT DATE 11 February 1981
		13. NUMBER OF PAGES 51 12 601
		15. SECURITY CLASS. (of this report) Unclassified
		15a. DECLASSIFICATION/DOWNGRADING SCHEDULE
16. DISTRIBUTION STATEMENT (of this Report) Approved for Public Release: Distribution Unlimited		
17. DISTRIBUTION STATEMENT (of the abstract entered in Block 20, if different from Report)		
18. SUPPLEMENTARY NOTES		
19. KEY WORDS (Continue on reverse side if necessary and identify by block number) V/STOL Lateral/Directional Characteristics Transition Inlet effects Jet induced effects		
20. ABSTRACT (Continue on reverse side if necessary and identify by block number) A method for estimating the power induced increments of side-force and yawing and rolling moments in the transition speed range is presented and compared with available data. The study shows that in addition to the expected inlet effects and the lateral shift in the induced downloads on the body and wing there is a large favorable sidewash induced at the vertical tail as well as suction pressures induced on the leeward side of the body that add significantly to the side-force and rolling and yawing moments.		

411340

TABLE OF CONTENTS

	Page
TABLE OF CONTENTS	ii
LIST OF FIGURES	iii
SYMBOLS	v
SUMMARY	1
INTRODUCTION	2
DEVELOPMENT OF THE METHOD	
Basis of the Method	3
Inlet	5
Body	6
Wing	13
Tail	15
COMPARISON WITH EXPERIMENTAL DATA	19
COMBINED ANGLES	22
CONCLUDING REMARKS	24
REFERENCES	25
APPENDIX: Sample Calculation	
Inlet	26
Body	27
Wing	28
Tail	28
TABLE I - GEOMETRIC CHARACTERISTICS OF CONFIGURATIONS	30

Accession For	
NTIS GRA&I	<input checked="" type="checkbox"/>
DTIC TAB	<input type="checkbox"/>
Unannounced	<input type="checkbox"/>
Justification	
Distribution/	
Available from Codes	
Dist	of
A	

LIST OF FIGURES

Figure	Title	Page
Development of Method		
1	Schematic of Effects of Sideslip on Jet Induced Pressures	4
2	Side-Force Factor K_y	7
3	Adjustment Factor for Nozzle Configuration	9
4	Schematic of Source of Rolling Moment Induced on Body	11
5	Lateral Shift of Induced Wind Download	14
6	Sidewash Induced at Vertical Tail	17
Comparison with Experimental Data		
7	Comparison of Estimate with Data for Configuration 1	
	a) Induced Increments	32
	b) Total Lateral/Directional Derivatives	33
8	Comparison of Estimate with Data for Configuration 2	
	a) Induced Increments	34
	b) Total Lateral/Directional Derivatives	35
9	Comparison of Estimate with Data for Configuration 3	
	a) Induced Increments	36
	b) Total Lateral/Directional Derivatives	37
10	Comparison of Estimate with Data for Configuration 4	
	a) Induced Increments	38
	b) Total Lateral/Directional Derivatives	39
11	Comparison of Estimate with Data for Configuration 5	
	a) Induced Increments	40
	b) Total Lateral/Directional Derivatives	41
12	Comparison of Estimate with Data for Configuration 6	
	a) Induced Increments	42
	b) Total Lateral/Directional Derivatives	43
13	Comparison of Estimate with Data for Configuration 7	
	a) Induced Increments	44
	b) Total Lateral/Directional Derivatives	45

14	Comparison of Estimate with Data for Configuration 10	
	a) Induced Increments	46
	b) Total Lateral/Directional Derivatives	47
15	Effect of Large Angles of Sideslip, Configuration 3 at Zero Angle of Attack.	48
16	Effect of Large Combined Angles	
	a) Configuration 2	49
	b) Configuration 4	50
	c) Configuration 8	51

SYMBOLS

The lateral/directional data are referred to the body-axis system

A_j	total jet exit area, m^2
b	wing span, m
C_n	yawing moment coefficient, power off
C_l	rolling moment coefficient, power off
C_Y	side-force coefficient, power off
d	diameter of individual jet, m
D_e	effective diameter of total jet area, m
d_e	effective diameter of exit area of local group of jets, m
ΔD	inlet-momentum drag, N
F_Y	side-force, N
ΔF_Y	side-force increment due to induced effects, N
K_Y	side-force factor for lateral profile area
$K_{Y,n}$	side-force factor for nozzle configuration
l	length of slot nozzle or of row of circular nozzles, m
ΔL	lift increment due to induced effects, N
M_x	rolling moment, Nm
ΔM_x	rolling moment increment due to induced effects, Nm
M_z	yawing moment, Nm
ΔM_z	yawing moment increment due to induced effects, Nm
q	free stream dynamic pressure
S_w	reference area, m^2
S_Y	lateral profile area, m^2
s	jet spacing, m

T	total jet thrust, N
V	velocity, m/sec.
V_e	effective velocity ratio $\sqrt{\frac{\rho_o V_o^2}{\rho_j V_j^2}}$
\dot{w}_i	inlet weight flow, N/sec.
\dot{w}_j	exit weight flow, N/sec.
w	width of slot nozzle or of row of circular nozzles, m
X	effective arm of induced lift from jet center, positive when the induced lift is ahead of the jet center, m
X_n	longitudinal distance from nozzle center to aerodynamic center of vertical tail, positive when nozzle is ahead of tail, m
X'	longitudinal distance of jet from moment reference point, positive when jet is ahead of moment reference point, m
X_c	longitudinal distance of quarter chord point of mean geometric chord from moment reference point, positive when quarter chord point is ahead of moment reference point, m
X_t	longitudinal distance of tail aerodynamic center from moment reference point, negative for tail behind moment reference point, m
Y_w	effective lateral shift of induced wing lift, m
Z_n	vertical distance from nozzle exit plane to aerodynamic center of vertical tail, positive when tail is above nozzle exit plane, m
Z_t	vertical distance from moment reference point to aerodynamic center of vertical tail, m
ΔZ	effective vertical arm of inlet momentum force above inlet face, m
α	angle of attack, deg.
β	sideslip angle, deg.
σ	sidewash angle, deg.
δn	jet deflection angle, deg.
ρ	density kg/m ³

Subscripts

b	body
o	free stream
i	inlet
j	jet
w	wing
f	frong jet(s)
r	rear jet(s)

SUMMARY

A method for estimating the power induced increments of side-force and yawing and rolling moments in the transition speed range is presented and compared with available data. The study shows that in addition to the expected inlet effects and the lateral shift in the induced downloads on the body and wing there is a large favorable sidewash induced at the vertical tail as well as suction pressures induced on the leeward side of the body that add significantly to the side-force and rolling and yawing moments. Although the method demonstrates consistency with the data from which it was derived the data base is too small to determine the extent of applicability and additional experimental data is needed to confirm or modify and refine the present method.

INTRODUCTION

In the transition between hovering and conventional flight the aerodynamic characteristics of jet and fan powered V/STOL aircraft can be significantly effected by the inlet and exit flows from the propulsion system. An empirical method for estimating the effects of these flows on the longitudinal characteristics is presented in reference 1.

In a crosswind or sideslip condition the induced flow field produced by the inlet and exit flows is asymmetrical with respect to the aircraft configuration and significant effects on the lateral/directional characteristics can be experienced. The present study uses available data to develop a method for estimating the lateral/directional induced effects in the transition speed range.

The method is an extension of, and is designed to be used in conjunction with, the method of reference 1, for estimating the longitudinal induced effects.

The present method is intended for use only in preliminary design work and to give a general indication of the effects of the primary configuration variables. The induced effects are a complex function of many configuration variables and the development of a V/STOL aircraft will require careful experimental investigations to accurately determine the induced forces and moments.

DEVELOPMENT OF THE METHOD

Basis of the Method:

The side-force and rolling and yawing moments acting on a V/STOL aircraft in transition can be considered to be made up of the sum of the power off forces and moments and the jet induced increments. For small sideslip angles:

$$\text{Side force, } F_Y = C_{Y,\beta} q S \beta + \left(\frac{\Delta F_Y}{T} \right) \beta T \beta$$

$$\text{Yawing Moment, } M_z = C_{n,\beta} q S b \beta + \left(\frac{\Delta M_z}{T D_e} \right) \beta T D_e \beta$$

$$\text{Rolling Moment, } M_x = C_{l,\beta} q S b \beta + \left(\frac{\Delta M_x}{T D_e} \right) \beta T D_e \beta$$

The induced increments, ΔF_Y , ΔM_z and ΔM_x are produced by pressures induced on the body, wing and tail by the inlet and exit flows. The pressures induced by the exit flows are illustrated schematically in figure 1. The download induced on the wing and body by the jet flux can be estimated by the method presented in reference 1. In a sideslip condition these downloads are shifted toward the leeward wing and produce a rolling moment. In addition the same jet wake vorticity and entrainment action that produces these downloads also induces suction pressures on the leeward side of the body and produce a sideforce and yawing moment. The vorticity also induces a sidewash at the vertical tail that produces a side force, rolling moment and yawing moment.

In addition the flow into the inlet will generate a side force (analogous to the inlet-momentum drag) and associated yawing and rolling moments. The total induced effects are the sum of these induced increments and can be written as:

$$\left(\frac{\Delta F_Y}{T} \right) \beta = \left(\frac{\Delta F_Y}{T} \right) \beta_{\text{inlet}} + \left(\frac{\Delta F_Y}{T} \right) \beta_{\text{body}} + \left(\frac{\Delta F_Y}{T} \right) \beta_{\text{tail}}$$

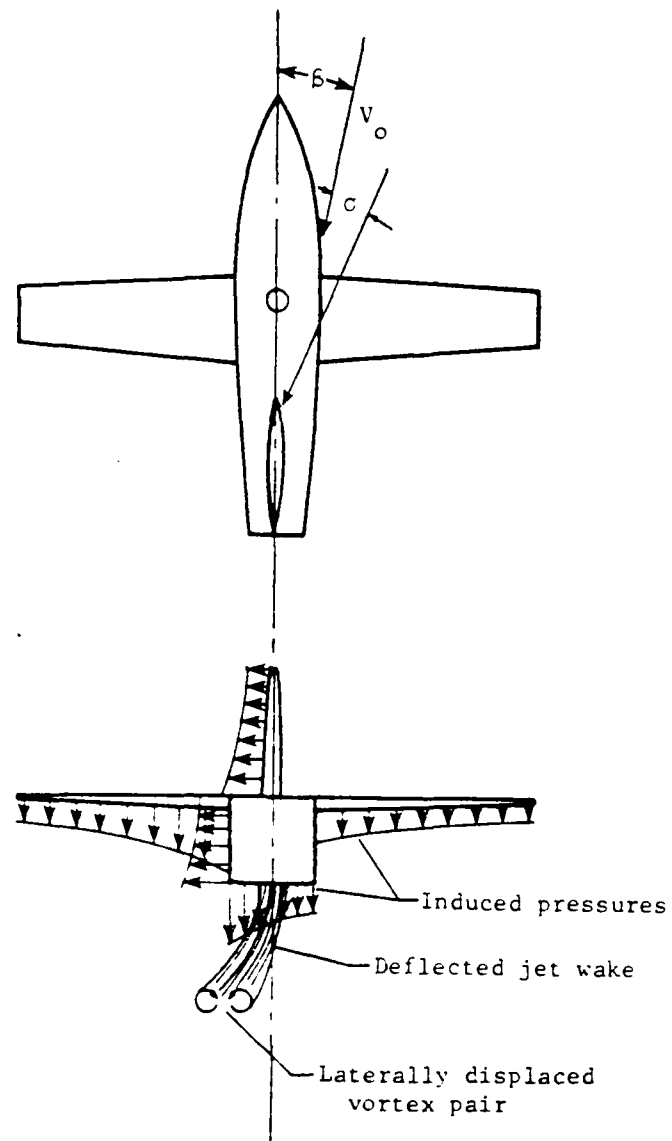


Figure 1.- Schematic of effect of side slip
on jet induced pressures.

$$\left(\frac{\Delta M_z}{TD_e}\right) \beta = \frac{\Delta M_z}{TD_e} \beta_{inlet} + \frac{\Delta M_z}{TD_e} \beta_{body} + \frac{\Delta M_z}{TD_e} \beta_{tail}$$

$$\frac{\Delta M_x}{TD_e} \beta = \frac{\Delta M_x}{TD_e} \beta_{inlet} + \frac{\Delta M_x}{TD_e} \beta_{body} + \frac{\Delta M_x}{TD_e} \beta_{tail} + \left(\frac{\Delta M_x}{TD_e}\right) \beta_{wing}$$

Methods for estimating each term have been developed in the present study and are presented in the following sections.

Inlet:

The side-force due to flow into the inlets is the inlet-momentum force produced by the crossflow velocity, $V \sin \beta$, and can be expressed as the inlet momentum drag (from ref. 1) multiplied by the sine of the sideslip angle:

$$\frac{\Delta F_Y}{T} = \frac{\Delta D}{T} \sin \beta = \frac{\dot{w}_i}{\dot{w}_j} V_e \sin \beta$$

and for small angles

$$\left(\frac{\Delta F_Y}{T}\right) \beta_{inlet} = -0.0175 \frac{\dot{w}_i}{\dot{w}_j} V_e$$

For a fan or jet engine the ratio of inlet to exit mass flow $\frac{\dot{w}_i}{\dot{w}_j}$ is equal to or

slightly less than unity. However some model experiments use ejectors to simulate the thrust producing devices and for these the actual ratio, which can be as low as 0.5, must be used.

The yawing and rolling moments due to turning the flow into the inlets is given by the side-force multiplied by the effective arm. For yawing moment the arm is the longitudinal distance from the moment reference point to the center of the inlet face, x_i , and:

$$\frac{\Delta M_z}{TD_e} \beta_{inlet} = \frac{\Delta F_Y}{T} \beta_{inlet} \frac{x_i}{D_e}$$

The rolling moment arm is the vertical distance to the effective center of action of the side-force increment due to the inlet flow. For forward facing inlets the arm is the vertical distance from the moment reference point to the center of the inlet face, Z_i .

For upper surface inlets the side-force (like the drag in the longitudinal mode, ref. 1) acts at a distance ΔZ above the inlet face. The rolling moment due to inlet flow is given by:

$$\frac{(\Delta M_x)}{TD_e} \beta_{\text{inlet}} = \frac{\Delta F_y}{T} \beta_{\text{inlet}} \frac{(Z_i + \Delta Z)}{D_e}$$

where $\Delta Z = .75d$ (ref. 1) and applies only to upper surface inlets.

For configurations with multiple inlets the side-force, yawing moment and rolling moment contributions of each must be calculated separately and summed.

Body:

The induced side-force due to the exiting flow is composed of two parts, the side-force induced on the body and the side-force due to the jet induced sidewash at the vertical tail. With the limited amount of data available it was necessary to iteratively examine various assumptions to determine and quantify the primary parameters that determine the magnitude of each contribution.

The available data indicates that the variation of jet induced side-force with effective velocity ratio, V_e , is similar to that of the lift-loss, $\frac{\Delta L}{T}$, of reference 1 and that the magnitude of the side-force increment increases as the size of the configuration relative to the jet exit area increases. It was determined that the body contribution to side-force could be adequately estimated for most configurations by multiplying the lift-loss as estimated from ref. 1 by a factor, K_y , that is a function of the ratio of

the lateral profile area of the configuration to the jet area, $\frac{S_y}{A_j}$, fig. 2.

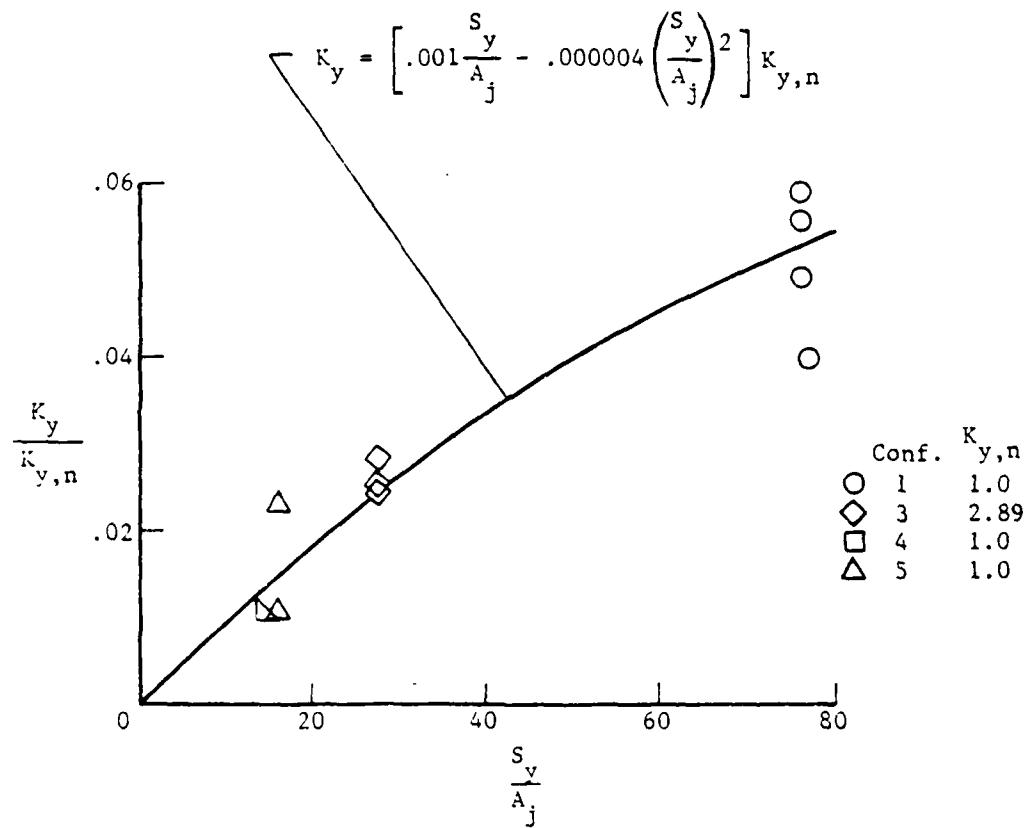


Figure 2.- Sideforce factor K_y .

However the data for configurations 3 and 8 were underestimated by this approach alone. Configuration 3 uses 2 rows of closely spaced jets and configuration 8 uses 3 jets in line in the nose of the body (approximating parallel slot jets) and the lift loss for these configurations is lower than it would be for the same configuration with a single round jet (see figure 27 of ref. 1). In the longitudinal mode the free stream flow is parallel to the rows of jets and the induced pressures are reduced. However, the crossflow component of the flow is perpendicular to the rows of jets and the position and strength of the vortex wake will be changed. Reference 2 indicates that a slot nozzle crosswise to the free stream induces significantly higher suction pressures than a streamwise slot or a round jet. To account for these higher induced pressures a nozzle side-force factor, $K_{Y,n}$, (figure 3) is introduced and is defined as the ratio of the adjustment factor for nozzle configuration (figure 16 of reference 1) for the slot perpendicular to the flow ($w/l > 1.0$) to the adjustment factor for the slot nozzle parallel to the flow ($w/l < 1.0$). It should be noted that this approach is based on a very limited data base and the factor $K_{Y,n}$ for slot nozzles (or rows of closely spaced jets) should be used with caution until the approach used here is verified or modified by additional data.

In the present method the body contribution to side-force, for small sideslip angles, can be estimated by:

$$\left(\frac{\Delta F_Y}{T} \right)_{\beta, \text{body}} = \left(\frac{\Delta L}{T} \right)_{\text{body}} K_Y$$

where $\left(\frac{\Delta L}{T} \right)_{\text{body}}$ is estimated by the method of reference 1,

$$K_Y = \left[.001 \frac{S_Y}{A_j} - .000004 \left(\frac{S_Y}{A_j} \right)^2 \right] K_{Y,n}$$

and $K_{Y,n}$ is obtained from figure 3.

The yawing moment induced on the body can be expressed as the side-force acting at an effective arm, X . It was found that the yawing moment arm is the same as the arm used in reference 1 for estimating the pitching moment associated with the induced lift loss. The yawing moment induced on the body can be estimated by:

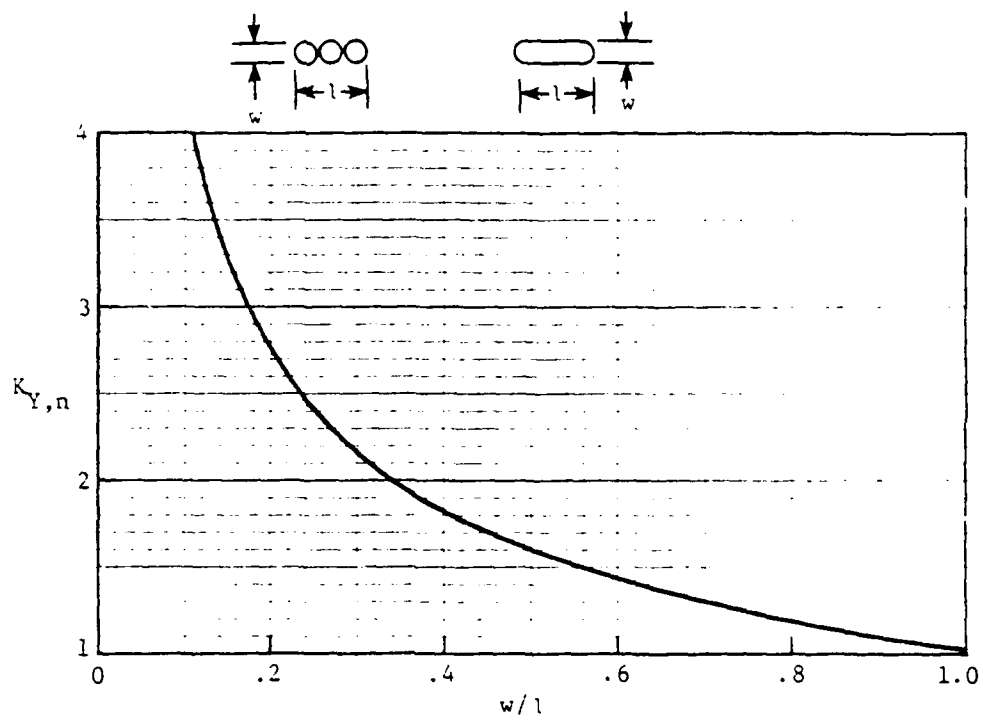


Figure 3.- Adjustment factor for nozzle configuration.

$$\left(\frac{\Delta M_z}{TD_e} \right)_{\beta, \text{body}} = \left(\frac{\Delta F_Y}{T} \right)_{\beta, \text{body}} \frac{X}{D_e}$$

where $\frac{X}{D_e}$ is obtained from reference 1.

The rolling moment induced on the body is associated with the lateral displacement of the pressure distribution induced on the lower surface of the body as indicated in figure 4. For jets within the body (fig. 4a) the rolling moment is given by:

$$\frac{\Delta M_x}{TD_e} = \left(\frac{\Delta L}{T} \right)_{\text{body}} \frac{X}{D_e} \sin \beta$$

and for small angles

$$\left(\frac{\Delta M_x}{TD_e} \right)_{\text{body}} = .0175 \left(\frac{\Delta L}{T} \right)_{\text{body}} \frac{X}{D_e}$$

where $\frac{X}{D_e}$ and $\left(\frac{\Delta L}{T} \right)_{\text{body}}$ are obtained from the method of ref. 1.

When the jets are located at the side of the body as indicated in figure 4b the induced lift loss on the leeward side is reduced but moved further from the moment reference point, and the induced lift loss on the upwind side is increased but moved closer to the moment reference point. There is no method available to estimate either the change in magnitude or the change in position of the induced lift but the two effects tend to cancel each other and, in the present method, the rolling moment induced on the body by jets at the side of the body is assumed to be zero.

Estimates for configurations with multiple jets distributed fore and aft of the moment reference point depend on the jet spacing. As indicated in reference 1, if the jet spacing is small, $\frac{s}{d} < 1.0$, the effects are similar to a slot nozzle and can be estimated as indicated above and in reference 1. For larger jet spacing the jet induced effects of the fore and aft jets, or groups of jets, are calculated separately and summed.

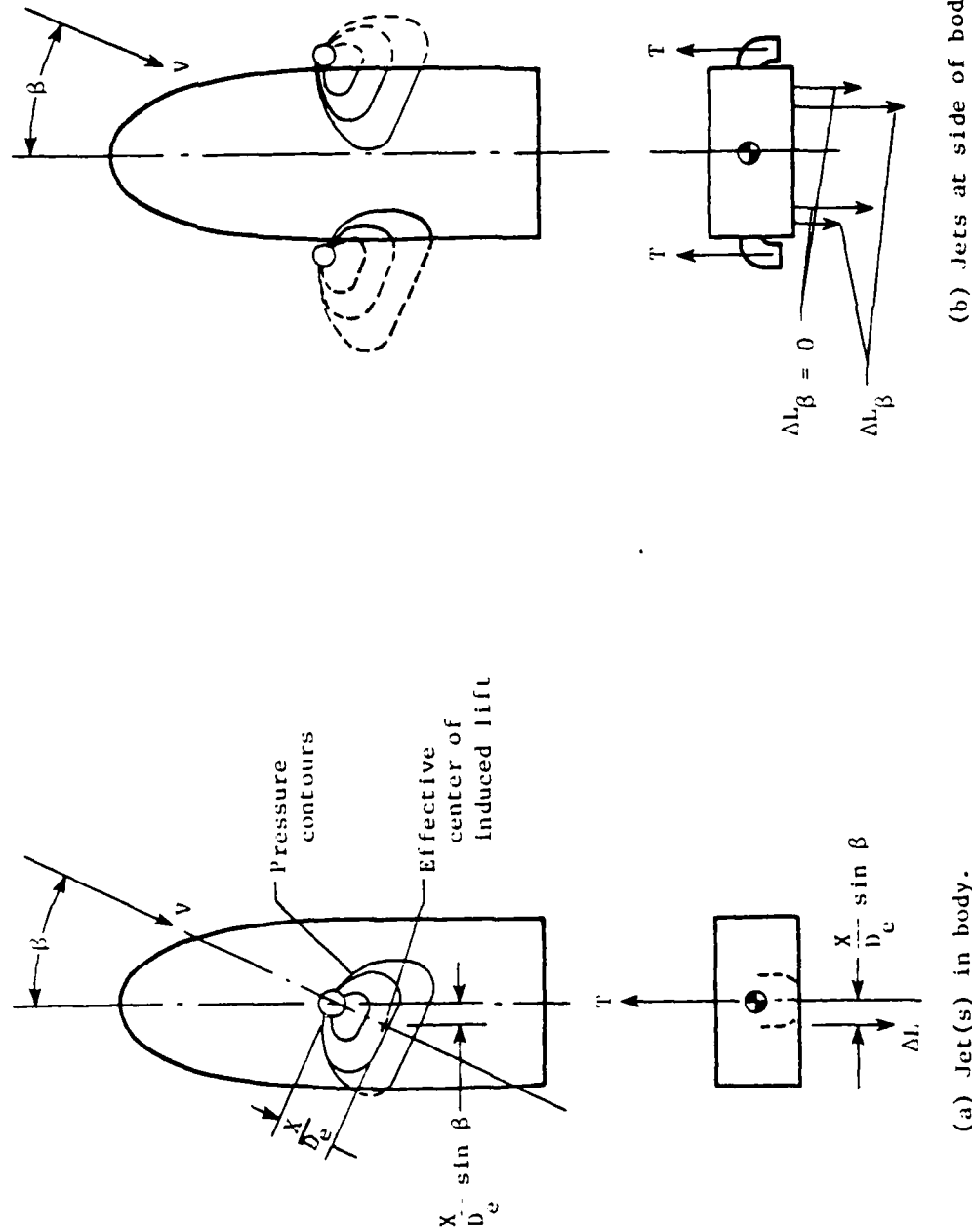


Figure 4.- Schematic of source of rolling moment induced on the body.

The side-force increment is given by:

$$\left(\frac{\Delta F_Y}{T} \right)_{\beta, \text{body}} = \left(\frac{\Delta L_f}{T} \right)_{\text{body}} K_Y + \left(\frac{\Delta L_r}{T} \right)_{\text{body}} K_Y$$

where $\left(\frac{\Delta L_f}{T} \right)_{\text{body}}$ and $\left(\frac{\Delta L_r}{T} \right)_{\text{body}}$ are the lift loss increments for

the front and rear groups of jets respectively as calculated by the method of reference 1.

The yawing moment and rolling moment increments are given by:

$$\left(\frac{\Delta M_z}{TD_e} \right)_{\beta, \text{body}} = \frac{\Delta L_f}{T} \text{body } K_Y \frac{X_f + X'_f}{D_e} + \left(\frac{\Delta L_r}{T} \right)_{\text{body}} K_Y \frac{X_r + X'_r}{D_e}$$

$$\text{and } \left(\frac{\Delta M_x}{TD_e} \right)_{\beta, \text{body}} = \frac{\Delta L_f}{T} \text{body } .0175 \frac{X_f}{D_e} + \left(\frac{\Delta L_r}{T} \right)_{\text{body}} .0175 \frac{X_r}{D_e}$$

where X_f and X_r are the effective arms of the lift induced by the front and rear groups of jets respectively as calculated by reference 1. Note that for a jet at or not too far ahead of the moment reference point the side-force acts behind the moment reference point producing a yawing moment increment that is stabilizing.

However if the jet spacing is large enough the side-force induced by the front jets can act ahead of the moment reference point and produce a destabilizing yawing moment contribution. The aft jets of course induce a stabilizing contribution. Most of the configurations for which tail off data are available indicate that the body contribution to yawing moment is stabilizing, however the data from configuration 8 indicates the body contribution to be destabilizing. Apparently the destabilizing contribution of the forward jets exceeds the stabilizing contribution of the rear jets. In fact analysis indicates that the best fit with the experimental data for configurations with the aft jets behind the wind (configurations 6, 7 and 8) is obtained by assuming the aft jets contribution to side-force, yawing moment and rolling moment are zero.

For configurations with the aft jets behind the wing (as in configurations 6, 7 and 8) the induced increments are given by:

$$\left(\frac{\Delta F_Y}{T} \right) \beta_{\text{body}} = \left(\frac{\Delta L_f}{T} \right)_{\text{body}} K_Y$$

$$\left(\frac{\Delta M_z}{TD_e} \right) \beta_{\text{body}} = \left(\frac{\Delta L_f}{T} \right)_{\text{body}} K_Y \frac{X_f + X'_f}{D_e}$$

$$\left(\frac{\Delta M_x}{TD_e} \right) \beta_{\text{body}} = \left(\frac{\Delta L_f}{T} \right)_{\text{body}} .0175 \frac{X_f}{D_e}$$

Wing:

The wing contribution to the induced rolling moment is caused by the lateral shift of the induced download on the wing. For a jet at the quarter chord point of the mean geometric chord of the wing (projected to the plane of symmetry) the lateral shift was found to be a function of the wing span (figure 5) and is 0.85 percent of the span per degree sideslip. For configurations with a jet or jets at a distance ahead of the quarter chord point the geometric lateral displacement of the wing with respect to the jet wake $((X' - X_c) \sin \beta)$ must also be accounted for. The data indicates that there is no rolling moment due to the favorable lift induced by jets at or behind the wing trailing edge.

The wing contribution to the rolling moment, for small side-slip angles, is given by:

$$\left(\frac{\Delta M_x}{TD_e} \right) \beta_{\text{wing}} = \left(\frac{\Delta L}{T} \right)_{\text{wing}} .0085 \frac{b}{D_e} + .0175 \frac{X' - X_c}{D_e}$$

where $\left(\frac{\Delta L}{T} \right)_{\text{wing}}$ is obtained from reference 1.

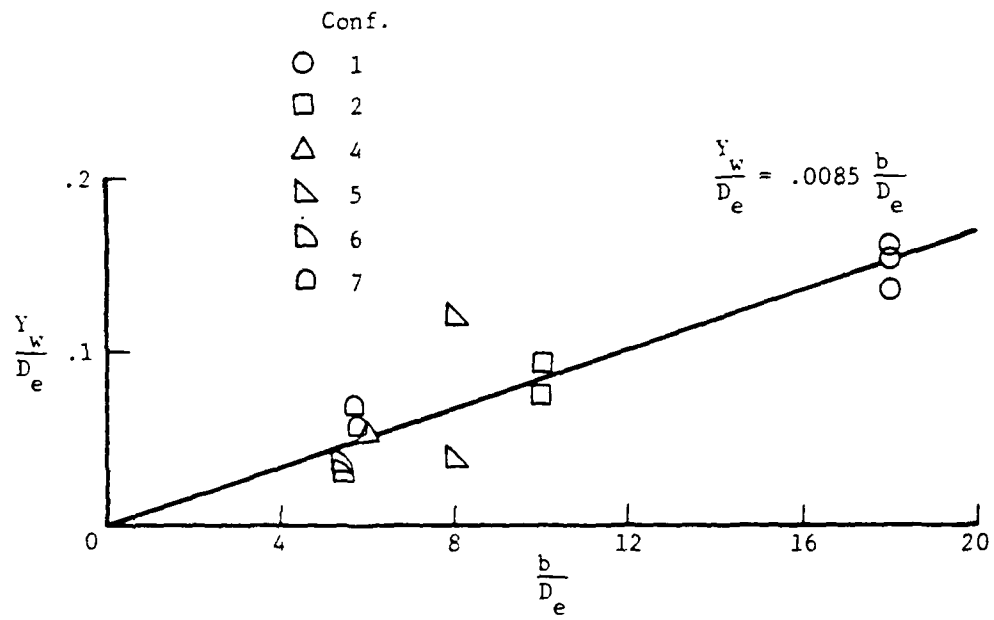


Figure 5.- Lateral shift of induced wing download, per degree β .

As indicated above for the body contributions, the effects of fore and aft distribution of the jets depends on the jet spacing. If the jet spacing is small, $\frac{s}{d} < 1.0$, the effects are similar to a slot nozzle and the factor $K_{Y,n}$ is applied:

$$\left(\frac{\Delta M_x}{TD_e} \beta_{wing} = \frac{\Delta L}{T} wing \left(.0085 \frac{b}{D_e} + .0175 \frac{X' - X_c}{D_e} \right) K_{Y,n} \right)$$

For a wider spacing the contribution of the front and rear jets must be calculated separately and summed.

$$\begin{aligned} \frac{\Delta M_x}{TD_e} \beta_{wing} &= \frac{\Delta L_f}{T} wing \left(.0085 \frac{b}{D_e} + .0175 \frac{X'_f - X_c}{D_e} \right) K_{Y,n,f} \\ &+ \frac{\Delta L_r}{T} wing \left(.0085 \frac{b}{D_e} + .0175 \frac{X'_r - X_c}{D_e} \right) K_{Y,n,r} \end{aligned}$$

And for configurations with the aft jets behind the wing only the front jets are assumed to contribute to the rolling moment:

$$\left(\frac{\Delta M_x}{TD_e} \beta_{wing} = \frac{\Delta L_f}{T} wing \left(.0085 \frac{b}{D_e} + .0175 \frac{X'_f - X_c}{D_e} \right) K_{Y,n,f} \right)$$

Tail:

The tail contribution to side-force, yawing moment and rolling moment is caused by the favorable sidewash induced at the vertical tail. The sidewash is produced primarily by the vorticity in the jet wake and would be expected to be inversely proportional to the distance of the vertical tail from the jet wake. In-as-much-as the location of the jet wake vorticity is not known the sidewash has been correlated with the distance from the nozzle exit as shown in figure 6. For configurations 2 and 5 the value of the sidewash parameter $\frac{\partial \sigma}{\partial s}$ correlated reasonably well with the inverse of the distance, however for configuration 3 the data indicated a very large sidewash (before dividing by $K_{Y,n}$). Apparently the same increased vorticity, or change in

vortex position associated with the 2 parallel rows of jets that produced the high level of body side-force also induces the high sidewash at the tail. When the sidewash parameter is divided by the nozzle side-force parameter $K_{Y,n}$, the correlation presented in figure 6 is obtained.

The side-force induced at the vertical tail is given by:

$$\left(\frac{\Delta F_Y}{T} \right)_{S, \text{tail}} = \Delta C_{Y, \beta, \text{tail}} \frac{\frac{c}{2} V_o^2 \frac{S_w}{A_j} \frac{\partial \sigma}{\partial \beta}}{\rho V_j^2} = \Delta C_{Y, \beta, \text{tail}} \frac{\partial \sigma}{\partial \beta} \frac{S_w}{2A_j} V_e^2$$

where $\Delta C_{Y, \beta, \text{tail}}$ is the power off side-force coefficient due to the tail and can be obtained from power off data or calculated by the USAF DATCOM method, (reference 3, section 5.3.1)

$$\frac{\partial \sigma}{\partial \beta} = .9 \left(\sqrt{\frac{1.0}{\left(\frac{X_n}{D_e} \right) \left(\frac{Z_n}{D_e} \right)}} \right) K_{Y,n}$$

and $K_{Y,n}$ is obtained from figure 3.

The effects of fore and aft distribution with small jet spacing, $\frac{s}{d} < 1.0$, are accounted for by the application of $K_{Y,n}$ as indicated above. For larger spacing the sidewash due to the front and rear jets must be calculated separately and summed. The sidewash is given by:

$$\frac{\partial \sigma}{\partial \beta} = .9 \left(\sqrt{\frac{1.0}{\left(\frac{X_{n,f}}{d_e} \right) \left(\frac{Z_{n,f}}{d_e} \right)}} \right) K_{Y,n,f} + \frac{V'_e}{V_e} .9 \left(\sqrt{\frac{1.0}{\left(\frac{X_{n,r}}{d_e} \right) \left(\frac{Z_{n,r}}{d_e} \right)}} \right) K_{Y,n,r}$$

where $X_{n,f}$, $Z_{n,f}$, $X_{n,r}$ and $Z_{n,r}$ are the longitudinal and vertical distances from the nozzle to the vertical tail for the front and rear nozzles respectively. And $d_{e,f}$ and $d_{e,r}$ are the effective diameters of the front and rear groups of nozzles respectively.

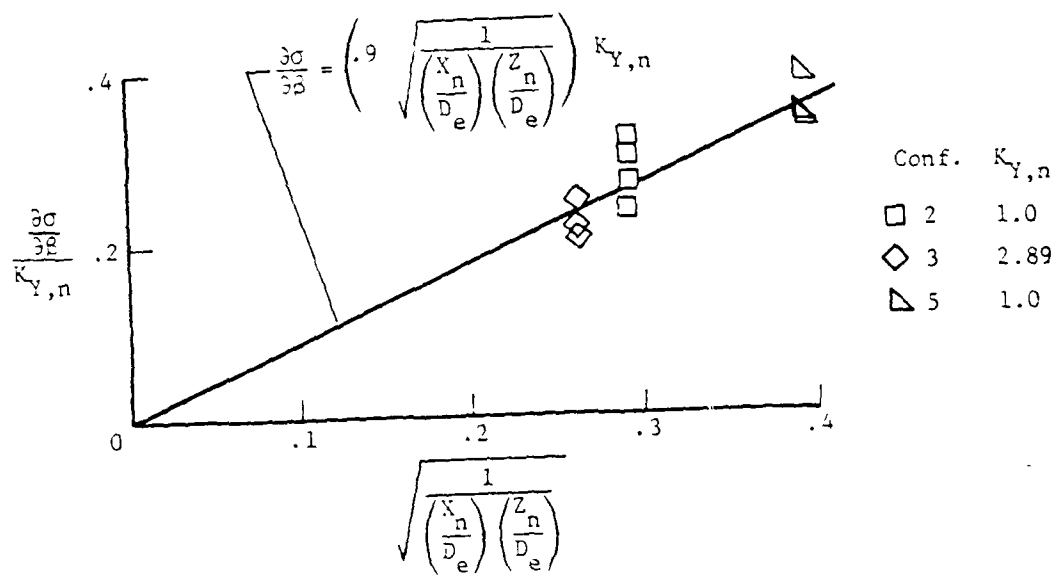
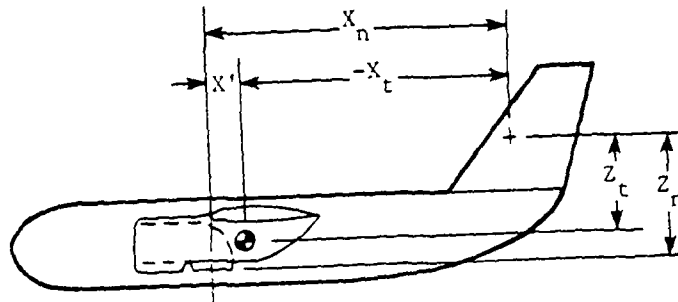


Figure 6.- Sidewash induced at vertical tail.

And $\frac{v'_e}{v_e} = \frac{\frac{s}{d} - 1.0}{\frac{s}{d} + .75}$ accounts for the reduced effectiveness of the rear jets

operating in the wake of the front jets.

For configurations with the aft jets behind the wing only the sidewash induced by the front jets is used:

$$\frac{\partial \sigma}{\partial \beta} = .9 \left(\sqrt{\frac{1.0}{\frac{x_{n,f}}{d_e} \left(\frac{z_{n,f}}{d_e} \right)}} \right) K_{Y,n,f}$$

The yawing moment increment due to the vertical tail is given by:

$$\left(\frac{\Delta M_x}{TD_e} \right)_{\beta, \text{tail}} = \left(\frac{\Delta F_Y}{T} \right)_{\beta, \text{tail}} \frac{x_t}{d_e}$$

The rolling moment increment due to the vertical tail is given by:

$$\left(\frac{\Delta M_x}{TD_e} \right)_{\beta, \text{tail}} = \left(\frac{\Delta F_Y}{T} \right)_{\beta, \text{tail}} \frac{z_t}{d_e}$$

COMPARISON WITH EXPERIMENTAL DATA

The power induced increments of side-force and rolling and yawing moment predicted by the method are compared with experimental data in figures 7 to 14. This is the same data set from which the method was developed and the comparison therefore demonstrates only the ability of the method to reproduce its source. However the comparisons also illustrate the relative significance of the various contributions.

The relatively simple wing-body single-jet configuration of reference 4 (configuration 1, figure 7) exhibits large induced increments of side-force and yawing and rolling moments because of the relatively large size of the configuration relative to the jet. (The configuration sketches in figures 7 to 14 are all drawn to the same scale relative to the equivalent jet diameter.) It is unfortunate that there is no wing off data available for configuration 1 to evaluate the assumption that the wing does not contribute to side-force and yawing moment and to evaluate the division of rolling moment between the wing and body.

A systematic investigation, varying jet size in a simple single-jet-in-body configuration is needed to evaluate and refine the variation of the side-force factor, K_Y (figure 2) with body size and to verify the assumption that the body contribution to rolling moment is given by $\frac{\Delta L}{T} \frac{X}{D_e} \sin \beta$

(figure 4). The same jet-in-body model could be used in a simple wing/body configuration to evaluate and refine the variation of lateral shift of wing

download, $\frac{Y_w}{D_e}$ (figure 5), with wing span to jet diameter ratio. A separate

investigation of the effects of jets beside the body is needed to provide a basis for estimating their contribution to the body and wing rolling moment increments.

One of the most interesting findings of the study is the determination that there is a significant favorable sidewash induced at the vertical tail. The experimental data indicated that the sidewash parameter $\frac{\partial \epsilon}{\partial \beta}$ can be as high as 0.35, that is the vertical tail effectiveness is increased by as much as

one third over the power off level. The downwash data presented in reference 2 (section 2.2.2.2) indicates that the jet induced downwash at the horizontal tail is a function of velocity ratio as well as vertical and longitudinal distance from the nozzle. Unfortunately there is insufficient data currently available to define these variations for the jet induced sidewash.

A systematic investigation varying the longitudinal and vertical distance of the tail from the jet exit is needed to evaluate and refine the method of estimating the sidewash factor (figure 6). The investigation should start with a single jet configuration and might use the same jet-in-body model suggested above for evaluating the side-force factor $K_{Y,n}$.

The estimated increments due to flow into the inlets are in relatively good agreement with the experimental data where experimental data are available (configurations 3, 4, and 5; figures 9, 10 and 11). The division of the weight flow between the top "blow-in-door" inlet and the forward facing inlets of configuration 2 (figure 8) is not available and therefore estimates could not be made. The inlet contribution shown in figure 8 is based on the experimental data rather than estimates.

It was noted in reference 1 that the additional vertical arm, Δz , for top inlets was based on the jet exit diameter ($\Delta z = .75d$) because the size of the inlets are generally not presented in the reports from which inlet effects can be extracted. Also there is considerable scatter in the data used in arriving at $\Delta z = .75d$ (reference 1). A systematic investigation to more accurately define Δz would be desirable.

It was noted earlier that the nozzle factor $K_{Y,n}$ was introduced to account for the high values of K_Y and $\frac{\partial \sigma}{\partial \beta}$ for configuration 3. The increase is assumed to be due to a change in strength and location of the jet wake vorticity from the parallel rows of closely spaced jets when operating in a sideslipping condition. Introduction of $K_{Y,n}$ is probably the weakest assumption in the present method. A systematic investigation of the effects of slot nozzles (or rows of closely spaced jets) is needed.

Configuration 8 (figure 14) exhibited a much larger jet induced increase in dihedral effect than any of the other configurations. Also the

jet induced yawing moment contribution of the body was destabilizing in contrast to the stabilizing contribution of the body for most of the other configurations. The directional instability contribution of the body could be accounted for by assuming that the rear jets had a negligible effect and therefore did not act to counter the destabilizing effects of the front jets. The same assumption of negligible contribution of jets located behind the wing results in reasonably good agreement between the estimates and experimental data for configurations 6 and 7 (fig. 12 and 13). However no method of accounting for the high induced dihedral effect on configuration 8 that is consistent with the rest of the method presented here could be found.

The method of handling tandem jet configurations, particularly those incorporated slot jets (or rows of jets as in configuration 8) needs further study including a systematic experimental investigation.

COMBINED ANGLES

The method developed above applies to small angles of sideslip at zero angle of attack. The data for 4 configurations extend to high angles of sideslip and three of these investigations also included the effects of angle of attack. Examples of these data are presented in figures 15 and 16 and compared with the estimates extended from small sideslip angles.

In general, at zero angle of attack the data is linear and the estimates are good out to sideslip angles of 6 to 10 degrees. At higher angles of sideslip, where separation effects are beginning to appear the experimental data falls below the linear extension of the small angle of sideslip estimate as would be expected.

The effects of angle of attack are generally small below about 10 degrees (and at sideslip angles below about 10 degrees) but become very large at high angles of attack where the wing is stalled. However, configuration 2 (figure 16 (a)) exhibits a significant reduction in dihedral effect when the angle of attack is increased from zero to 10 degrees. The power off data for this configuration indicate that the outer wing panels are beginning to stall at about 5 degrees angle of attack. At 10 degrees angle of attack the variation of lift with angle of attack is considerably lower than at zero and therefore the increment of rolling moment due to the different angles of attack induced on the leeward and windward wings by the jets effects would be expected to be reduced.

Configuration 4 (figure 16 (b)) however exhibits the opposite behavior. As expected the dihedral effect increases with angle of attack but the increase is much greater than would be expected due to power off sweep effects and extends to high sideslip angles. The reasons for this behavior are not obvious. This configuration also exhibits a dihedral effect reversal at small angles of sideslip at the lowest velocity ratio investigated (insert at top of figure 10). And at the highest velocity ratios the experimental increments of side-force, yawing moment and rolling moment all depart significantly from the predicted trend (figure 10). The reasons for these departures and reversals are not known but it should be noted that this configuration has a large negative geometric dihedral and the largest wing

NADC-81031-60

sweep of the configurations studied. These results suggest the need for additional investigation of the effects of dihedral angle and wing sweep on the jet induced effects.

CONCLUDING REMARKS

This study of the lateral/directional characteristics of V/STOL aircraft in the transition speed range has shown that in addition to the inlet effects and the lateral shift of the downloads induced on the body and wing in a sideslipping condition there is a large favorable sidewash induced at the vertical tail as well as suction pressures induced on the leeward side of the body that add significantly to the side-force and rolling and yawing moments.

The method developed in this study has demonstrated consistency with the data from which it was derived, however the data base is so small that the extent of applicability is unknown. Additional experimental data is needed to confirm or modify and refine the present method.

REFERENCES

1. Kuhn, Richard E., "An Empirical Method for Estimating the Jet-Induced Effects on V/STOL Configurations in Transition," Report No. R-AMPAC-113, Nov. 1979.

The essential parts of this paper are also included in reference 2.
2. Henderson, C., Clark, J. and Walters, M., "V/STOL Aerodynamics and Stability and Control Manual," NADC Rpt. No. NADC-80017-60, Jan. 1980.
3. Weston, R. P. and Thames, F. C., "Properties of Aspect-Ratio-4.0 Rectangular Jets in a Subsonic Crossflow," AIAA Journal of Aircraft, Vol. 16, No. 10, Oct. 1979, page 701.
4. "USAF Stability and Control Datcom," Oct. 1960, revised Jan. 1975.
5. Mineck, R. E., and Schwendemann, M. F., "Aerodynamic Characteristics of a Vectored-Thrust V/STOL Fighter in the Transition-Speed Range," NASA TN-D-7191, May 1973.
6. Vogler, R. D. and Kuhn, R. E., "Longitudinal and Lateral Stability Characteristics of Two Four-Jet FTOL Models in the Transition Speed Range," NASA TM-X-1092, May 1965.
7. Winston, Matthew, M., "Induced Interference Effects on the Aerodynamic Characteristics of a 0.16 Scale Sic-Jet V/STOL Model in Transition," NASA TN-D-5727, March 1970.
8. Winston, Matthew, M., "Wind-Tunnel Data from a 0.16-Scale V/STOL Model with Direct-Lift and Lift-Cruise Jets," NASA TM-X-1758, March 1969.
9. Margason, R. J. and Vogler, R. D., "Wind-Tunnel Investigation at Low Speeds of a Model of the Kestrel (XV-6A) Vectored-Thrust V/STOL Airplane," NASA TN-D-6826, July 1972.
10. Gambucci, B. J., Aoyagi, K. and Rolls, S. L., "Wind-Tunnel Investigation of a Large-Scale Model of a Lift/Cruise Fan V/STOL Aircraft with Extended Lift/Cruise Nacelles," NASA TM-X-73,164, Aug. 1976.
11. Hall, L. P., Hickey, D. H. and Kirk, J. V., "Aerodynamic Characteristics of a Large-Scale V/STOL Transport Model with Lift and Lift-Cruise Fans," NASA TN-D-4092, Aug. 1967.
12. Margason, R. J. and Gentry, G. L. Jr., "Aerodynamic Characteristics of a Five-Jet VTOL Configuration in the Transition Speed Range," NASA TN D-4812, Oct. 1968.

APPENDIX

Sample Calculation

The calculations for configuration 4 are presented in this section to illustrate the application of the method.

Inlet:

$$\left(\frac{\Delta F_Y}{T}\right)_{\beta, \text{inlet}} = -.0175 \frac{\dot{w}_i}{\dot{w}_j} v_e \quad \frac{\dot{w}_i}{\dot{w}_j} = .5$$

$$\left(\frac{\Delta M_z}{TD_e}\right)_{\beta, \text{inlet}} = \left(\frac{\Delta F_Y}{T}\right)_{\beta, \text{inlet}} \frac{X_i}{D_e} \quad \frac{X_i}{D_e} = 2.55$$

$$\left(\frac{\Delta M_x}{TD_e}\right)_{\beta, \text{inlet}} = \left(\frac{\Delta F_Y}{T}\right)_{\beta, \text{inlet}} \frac{Z_i}{D_e} \quad \frac{Z_i}{D_e} = 0$$

v_e	$\left(\frac{\Delta F_Y}{T}\right)_{\beta, \text{inlet}}$	$\left(\frac{\Delta M_z}{TD_e}\right)_{\beta, \text{inlet}}$	$\left(\frac{\Delta M_x}{TD_e}\right)_{\beta, \text{inlet}}$
.1	-.00087	-.00222	0
.2	-.00175	-.00445	0
.3	-.00262	-.00668	0

This configuration has only one forward facing inlet location. For configurations such as 3, 5, 7 and 8 the side-force, yawing moment and rolling moment contributions of each inlet must be calculated separately and summed.

The actual weight flow ratio used in the model tests is used in this calculation to provide a comparison with the model results. If the calculations were being made to estimate the characteristics of an airplane the weight flow ratio appropriate to the engine installation would be used.

Body:

$$\left(\frac{\Delta F_Y}{T}\right) \beta, \text{body} = \left(\frac{\Delta L_f}{T}\right) \text{body } K_Y + \left(\frac{\Delta L_r}{T}\right) \text{body } K_Y$$

where $\frac{\Delta L_f}{T}$ and $\frac{\Delta L_r}{T}$ are calculated by the method of reference 1 and

$$K_Y = \left[.001 \frac{S_Y}{A_j} - .000004 \left(\frac{S_Y}{A_j} \right)^2 \right] K_{Y,n} = .015$$

$$\frac{S_Y}{A_j} = 16$$

$$\begin{aligned} \left(\frac{\Delta M_z}{TD_e}\right) \beta, \text{body} &= \left(\frac{\Delta L_f}{T}\right) \text{body } K_Y \left(\frac{X+X'}{D_e}\right)_f \\ &+ \left(\frac{\Delta L_r}{T}\right) \text{body } K_Y \left(\frac{X+X'}{D_e}\right)_r \end{aligned}$$

$$\frac{W}{l} = 1.0$$

$$K_{Y,n} = 1.0$$

$$\left(\frac{X'}{D_e}\right)_f = .835$$

$$\left(\frac{X'}{D_e}\right)_r = -.835$$

$$\text{where } \left(\frac{X}{D_e}\right)_f = -2.068$$

$$\left(\frac{X}{D_e}\right)_r = -1.69$$

from method of
reference 1

$$\left(\frac{\Delta M_x}{TD_e}\right) \beta, \text{body} = 0 \quad (\text{jets at side of body})$$

v_e	$\left(\frac{\Delta L_f}{T}\right) \text{body}$	$\left(\frac{\Delta L_r}{T}\right) \text{body}$	$\left(\frac{\Delta F_Y}{T}\right) \beta, \text{body}$	$\left(\frac{\Delta M_z}{TD_e}\right) \beta, \text{body}$	$\left(\frac{\Delta M_x}{TD_e}\right) \beta, \text{body}$
.1	-.0144	-.0031	-.00026	.0004	0
.2	-.0617	-.0069	-.0010	.0016	0
.3	-.1044	-.0164	-.0018	.0025	0

For configurations in which the rear jets are behind the wing only the contribution of the front jets is used.

Wing:

$$\left(\frac{\Delta M_x}{TD_e}\right)_{\beta, \text{wing}} = \left(\frac{\Delta L_f}{T}\right)_{\text{wing}} \left(\frac{Y_w}{D_e} + .0175 \left(\frac{X' - X_c}{D_e}\right)_f\right) + \left(\frac{\Delta L_r}{T}\right)_{\text{wing}} \left(\frac{Y_w}{D_e} + .0175 \left(\frac{X' - X_c}{D_e}\right)_r\right)$$

$$\frac{Y_w}{D_e} = .0085 \frac{b}{D_e} = .0515$$

$$\frac{b}{D_e} = 6.06$$

v_e	$\left(\frac{\Delta L_f}{T}\right)_{\text{wing}}$	$\left(\frac{\Delta L_r}{T}\right)_{\text{wing}}$	$\left(\frac{\Delta M_x}{TD_e}\right)_{\beta, \text{wing}}$
.1	-.0152	-.0044	-.0013
.2	-.061	-.0110	-.0051
.3	-.0865	-.0303	-.0079

$$\left(\frac{X' - X_c}{D_e}\right)_f = 1.365$$

$$\left(\frac{X' - X_c}{D_e}\right)_r = -.305$$

For configurations in which the rear jets are behind the wing only the contribution of the front jets is used.

Tail:

$$\left(\frac{\Delta F_Y}{T}\right)_{\beta, \text{tail}} = \Delta C_{Y, \beta, \text{tail}} \frac{\partial \sigma}{\partial \beta} \frac{S_w}{2A_j} v_e^2$$

$$\frac{S_w}{2A_j} = 8.3$$

$$\Delta C_{Y, \beta, \text{tail}} = -.00692 \quad (\text{from power-off test data})$$

$$\left(\frac{X_n}{d_e}\right)_f = 8.66$$

$$\frac{\partial \sigma}{\partial \beta} = \left(\frac{\partial \sigma}{\partial \beta}\right)_f + \frac{v'_e}{v_e} \left(\frac{\partial \sigma}{\partial \beta}\right)_r$$

$$\left(\frac{Z_n}{d_e}\right)_f = 1.26$$

$$= .9 \sqrt{\frac{1.0}{\left(\frac{X_n}{d_e}\right)_f \left(\frac{Z_n}{d_e}\right)_f}} + \frac{v'_e}{v_e} .9 \sqrt{\frac{1.0}{\left(\frac{X_n}{d_e}\right)_r \left(\frac{Z_n}{d_e}\right)_r}} = 0.41$$

$$\left(\frac{X_n}{d_e}\right)_r = 6.30$$

$$\left(\frac{Z_n}{d_e}\right)_r = 1.26$$

$$\frac{s}{d} = 2.34$$

$$\frac{v'_e}{v_e} = \frac{\frac{s}{d} - 1.0}{\frac{s}{d} + .75} = 0.43$$

$$\left(\frac{\Delta M_z}{TD_e} \right) \beta_{\text{tail}} = \left(\frac{\Delta F_Y}{T} \right) \beta_{\text{tail}} \frac{x_t}{D_e}$$

$$\left(\frac{\Delta M_x}{TD_e} \right) \beta_{\text{tail}} = \left(\frac{\Delta F_Y}{T} \right) \beta_{\text{tail}} \frac{z_t}{D_e}$$

$$\text{where } \left. \begin{array}{l} \frac{x_t}{D_e} = -.529 \\ \frac{z_t}{D_e} = .8 \end{array} \right\} \text{from power off data}$$

v_e	$\left(\frac{\Delta F_Y}{T} \right) \beta_{\text{tail}}$	$\left(\frac{\Delta M_z}{TD_e} \right) \beta_{\text{tail}}$	$\left(\frac{\Delta M_x}{TD_e} \right) \beta_{\text{tail}}$
.1	-.0002	.0013	-.0002
.2	-.0009	.0050	-.0007
.3	-.0021	.0113	-.0017

If power-off data are not available $\frac{x_t}{D_e}$, $\frac{z_t}{D_e}$ and $LC_{Y,\beta_{\text{tail}}}$ can be calculated from geometry and the method of reference 3, section 5.3.1.

TABLE I
GEOMETRIC CHARACTERISTICS

Conf.	Ref.	Fig.	d cm	D _e cm	$\frac{b}{D_e}$	$\frac{S_w}{A_j}$	$\frac{S_y}{A_j}$	$\frac{w_i}{w_j}$	$\frac{X'}{D_e}$	$\frac{X_c}{D_e}$
1	5	7	5.72	5.72	17.9	81.4	76.3	-	0	-1.38
2	6	8	8.64	17.3	10.2	18.0	27.0	1.0	.68/-1.26*	-1.1
3	7,8	9	4.87	11.9	10.2	22.1	27.4	.5	-.23	-.27
4	9	10	9.6	19.2	6.06	16.6	16.0	.5	.835/-.835	-.53
5	5	11	9.32	13.2	7.75	15.3	14.3	.5	0	-.26
6	10	12	91.4	158	5.48	8.5	5.4	1.0	2.64/ -	0
7	11	13	91.4	182.8	6.08	8.2	5.8	1.0	1.42/ -	0
8	12	14	5.08	11.4	10.7	22.9	21.0	.5	1.78/ -	0

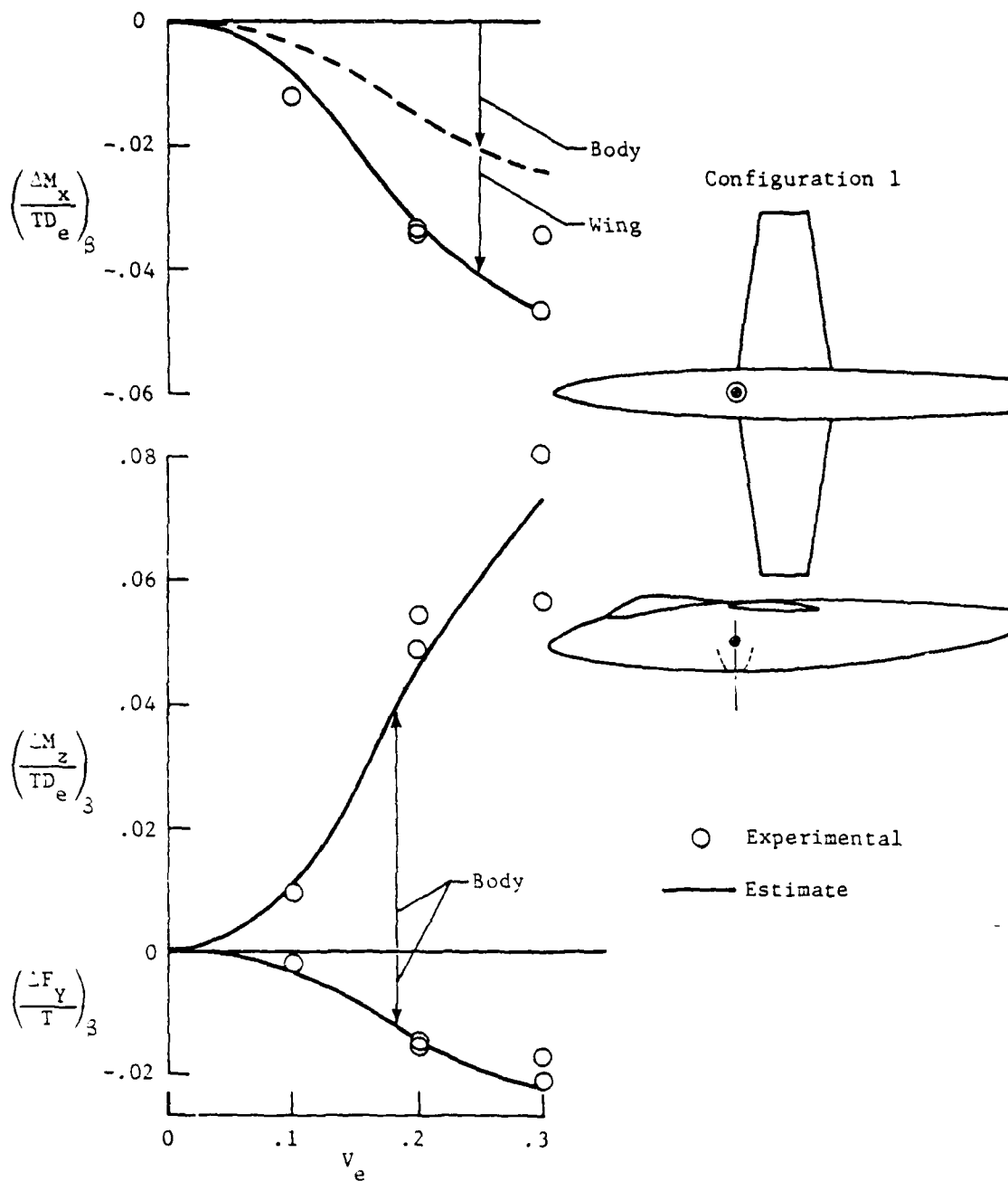
*front/rear

TABLE I
Concluded

Conf.	Forward facing inlet		Top inlet		$\frac{w}{t}$	$\frac{s}{d}$	$\frac{X_t}{D_e}$	$\frac{Z_t}{D_e}$	$\frac{X_n}{d_e}$	$\frac{Z_n}{d_e}$	Conf. No. in Ref. 1
	$\frac{X_i}{D_e}$	$\frac{Z_i}{D_e}$	$\frac{X_i}{D_e}$	$\frac{Z_i}{D_e}$							
1	-				1.0	-	-	-	-	-	2b
2	5.4	-.47	n.a.	n.a	1.0	2.89	-6.29	1.34	9.86* /.711	2.6	18a
3	2.07	.54	-.46	1.08	.186	-	-5.69	1.64	5.69	2.56	8
4	2.55	0	-	-	1.0	2.34	-5.29	.80	8.66 /6.30	.39	17
5	1.62	.16	-	-	1.0	-	-3.61	1.34	3.61	1.65	11a
6	.69	0	2.54	0	1.0	-	-1.85	.73	7.78 /-	1.89 /-	14
7	-	-	1.42* /.93	.422	1.0	-	-2.92	1.0	6.14 /-	.817 /-	13b
8	2.73	0	1.78	.67	.20	-	-5.31	.89	9.15 /-	2.02 /-	10b

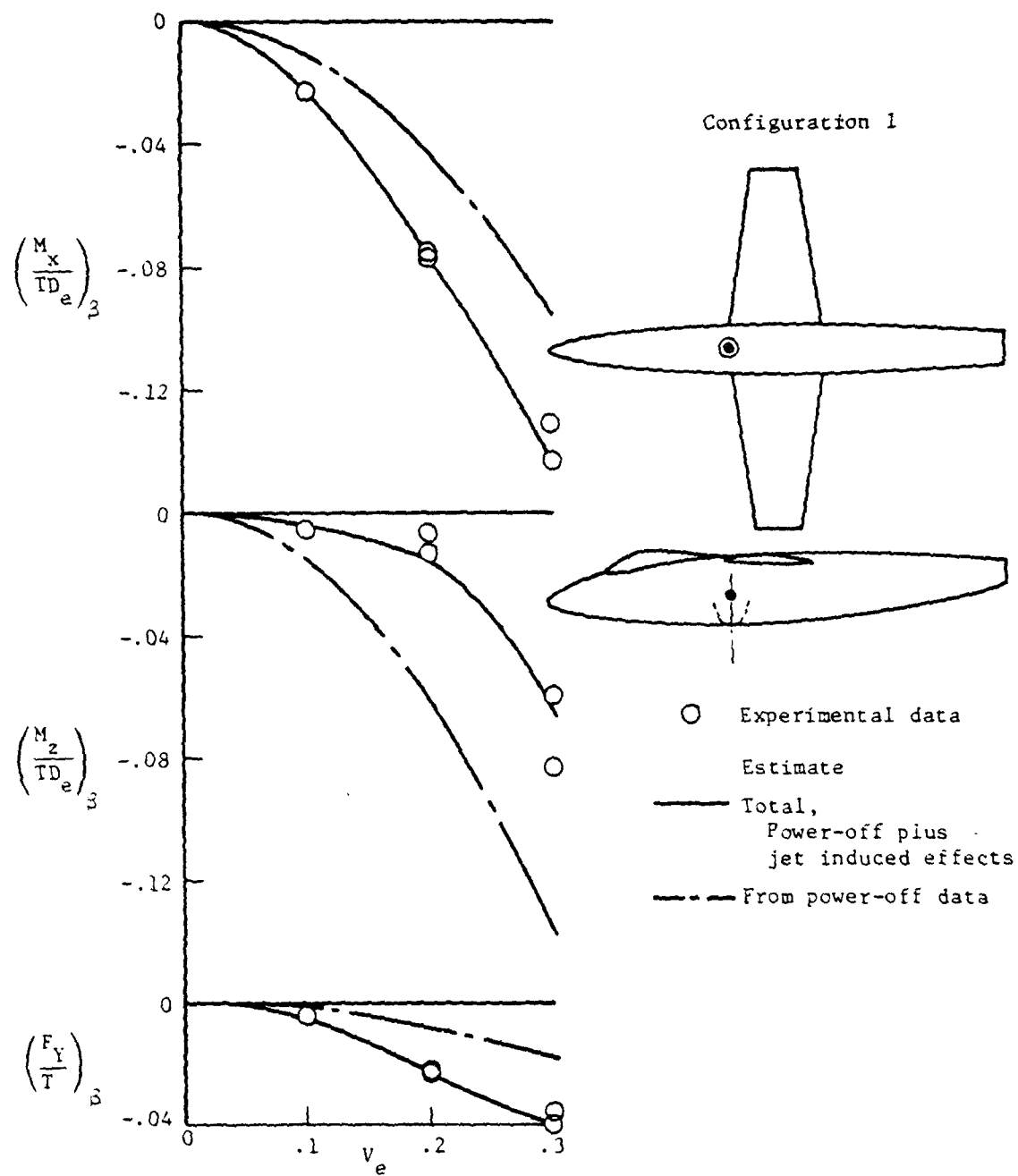
*front/rear

n.a. not available



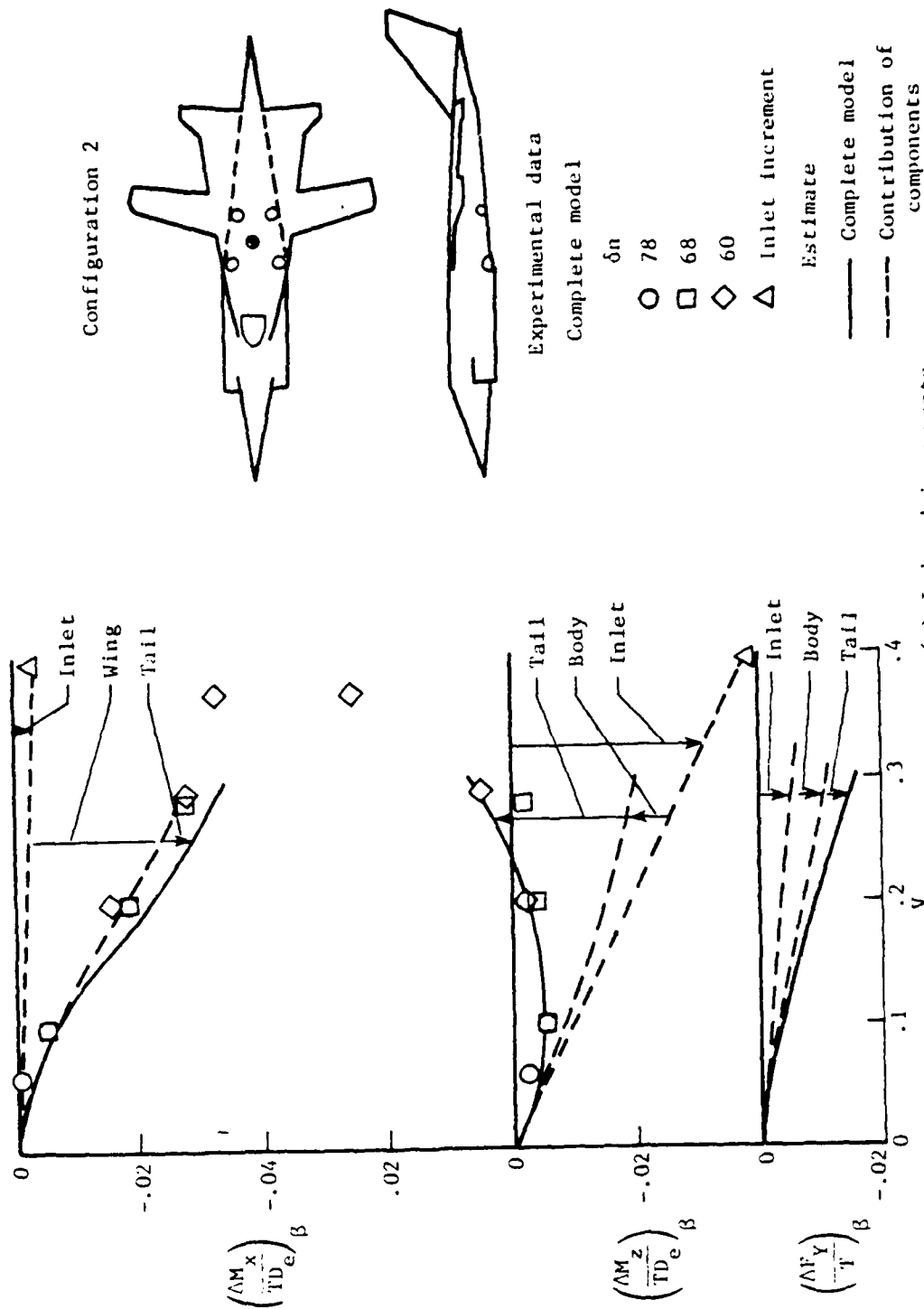
(a) Induced increments.

Figure 7.- Comparison of estimate with data for single jet configuration 1
(ref. 5) (Configuration 2b of ref. 1) $\left(\frac{w_i}{w_j} = 0\right)$



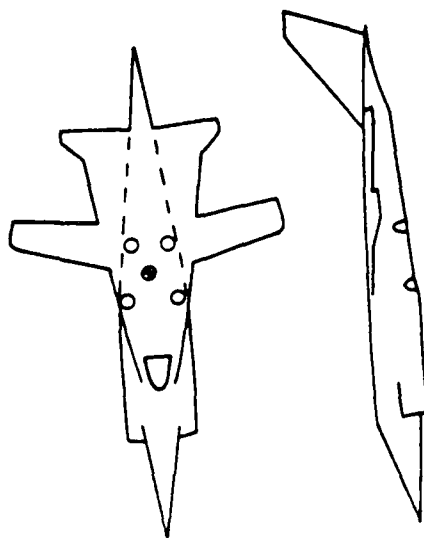
(b) Total lateral/directional derivatives

Figure 7.- Concluded.



(a) Induced increments.
 Figure 8.- Comparison of estimate with data for configuration 2 (ref. 6).
 (Configuration 18a of ref. 1) $\left(\frac{\dot{w}_1}{\dot{w}_j} = 1.0\right)$

Configuration 2



Experimental data

δ_n

○ 78

□ 68

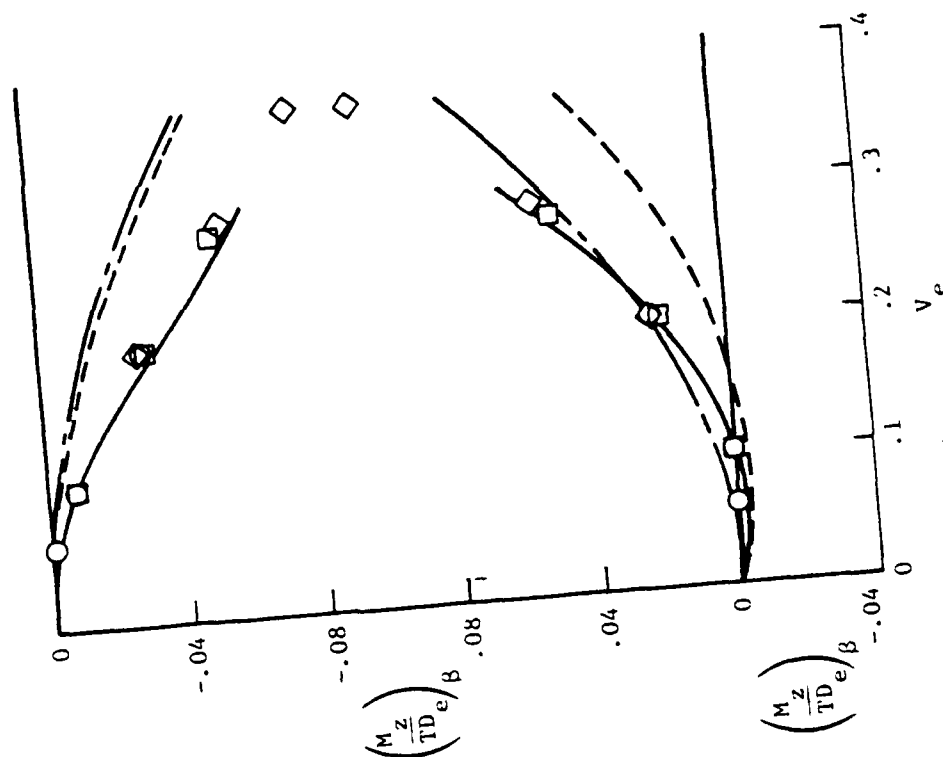
◇ 60

Estimates

— Total, power-off plus inlet and jet interference effects

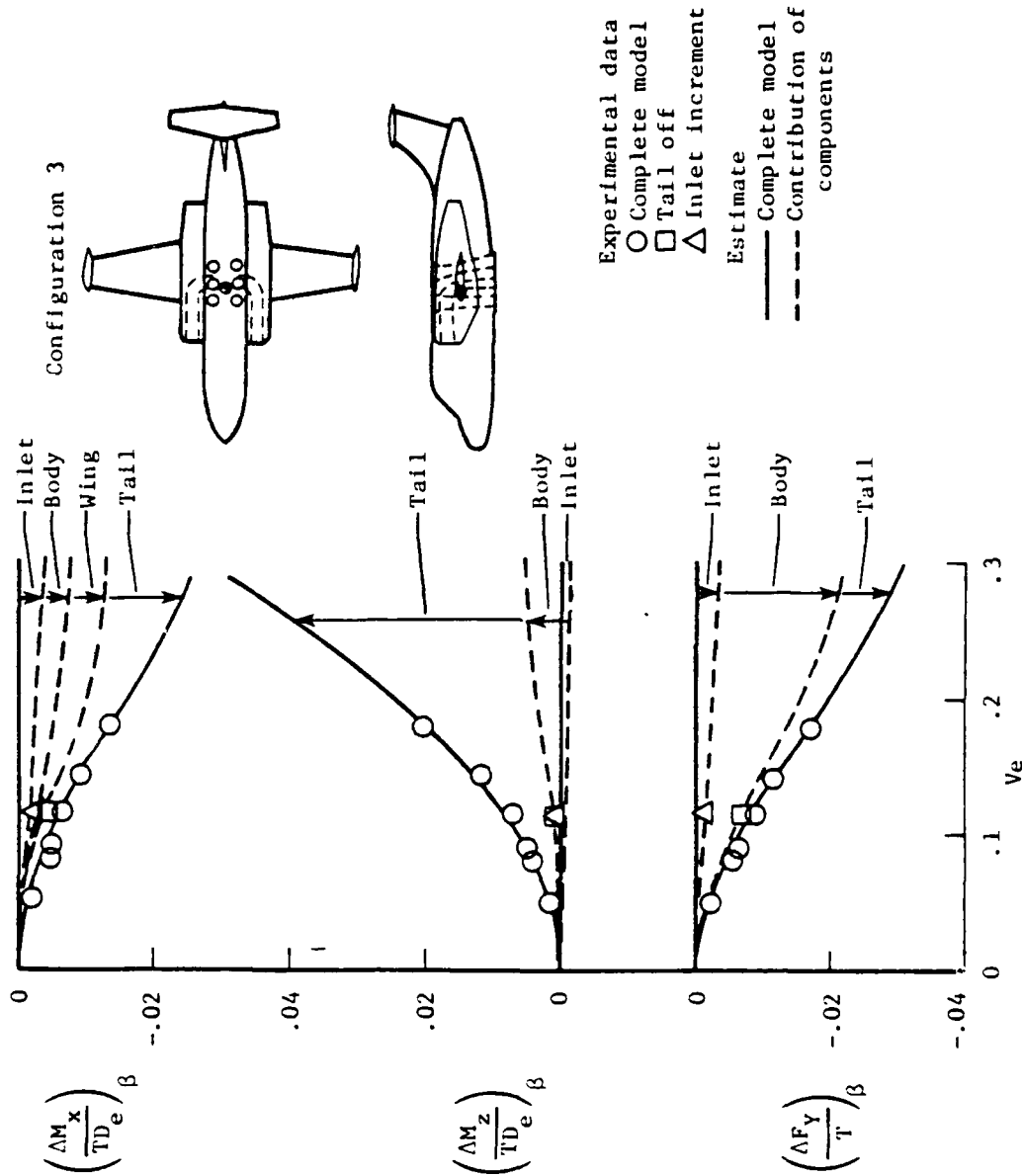
--- From power-off data

--- Power-off plus inlet



(b) Total lateral/directional derivatives.

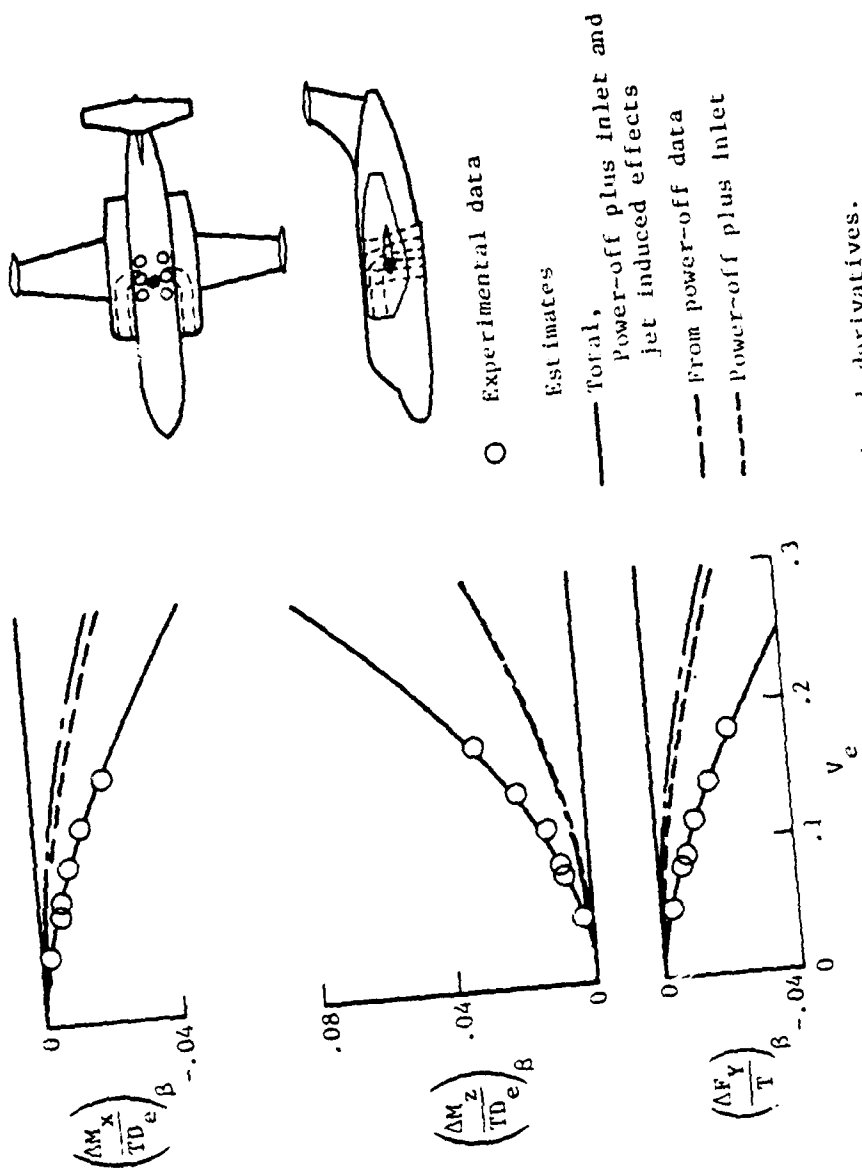
Figure 8.- Concluded.



(a) Induced increments.

Figure 9.- Comparison of estimate with data for Configuration 3 (ref. 7 & 8)
 (Configuration 8 of ref. 1) $\left(\frac{w_i}{w_j} = .5\right)$

Configuration 3



(b) Total lateral directional derivatives.
Figure 9.- Concluded.

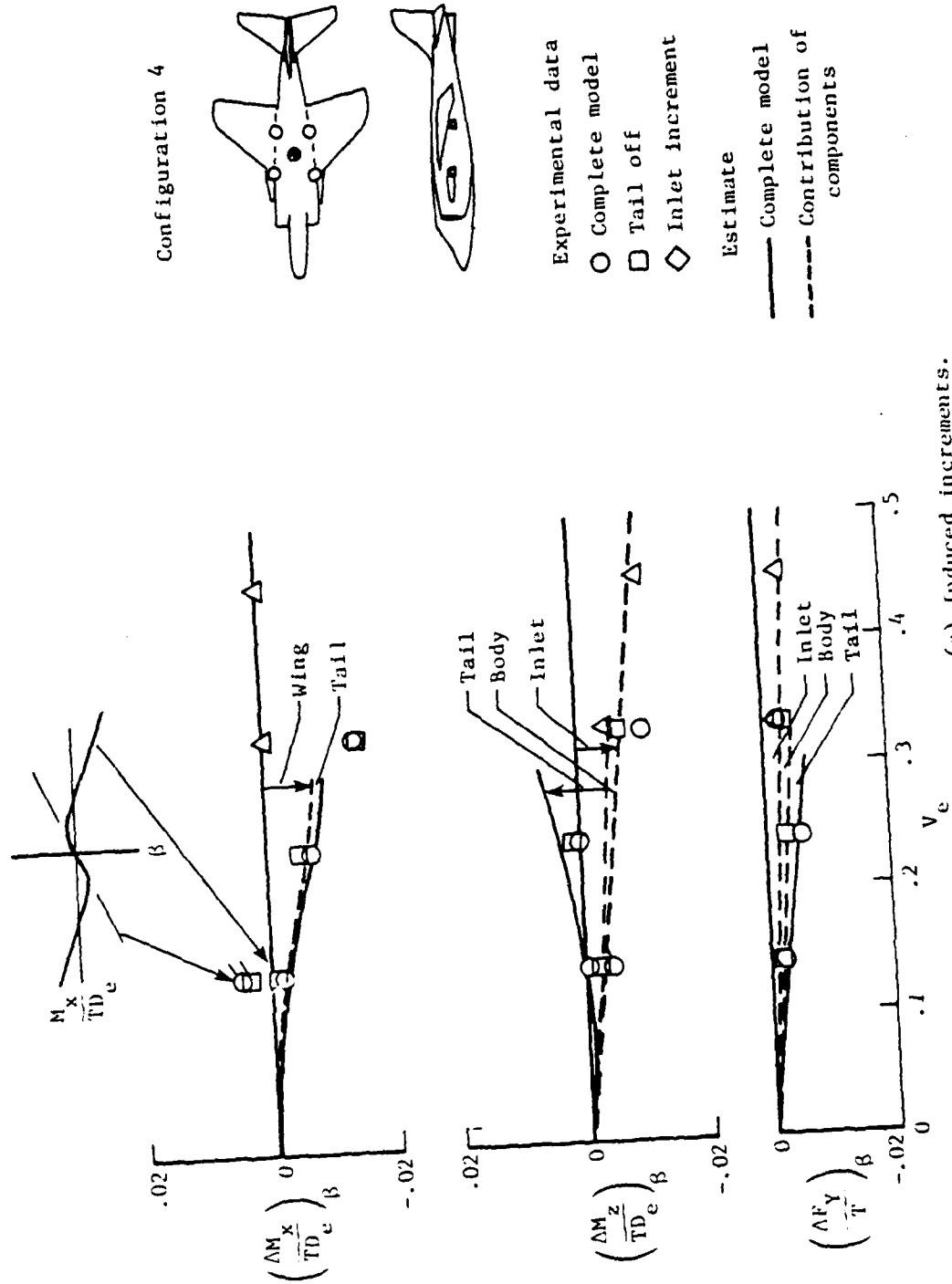
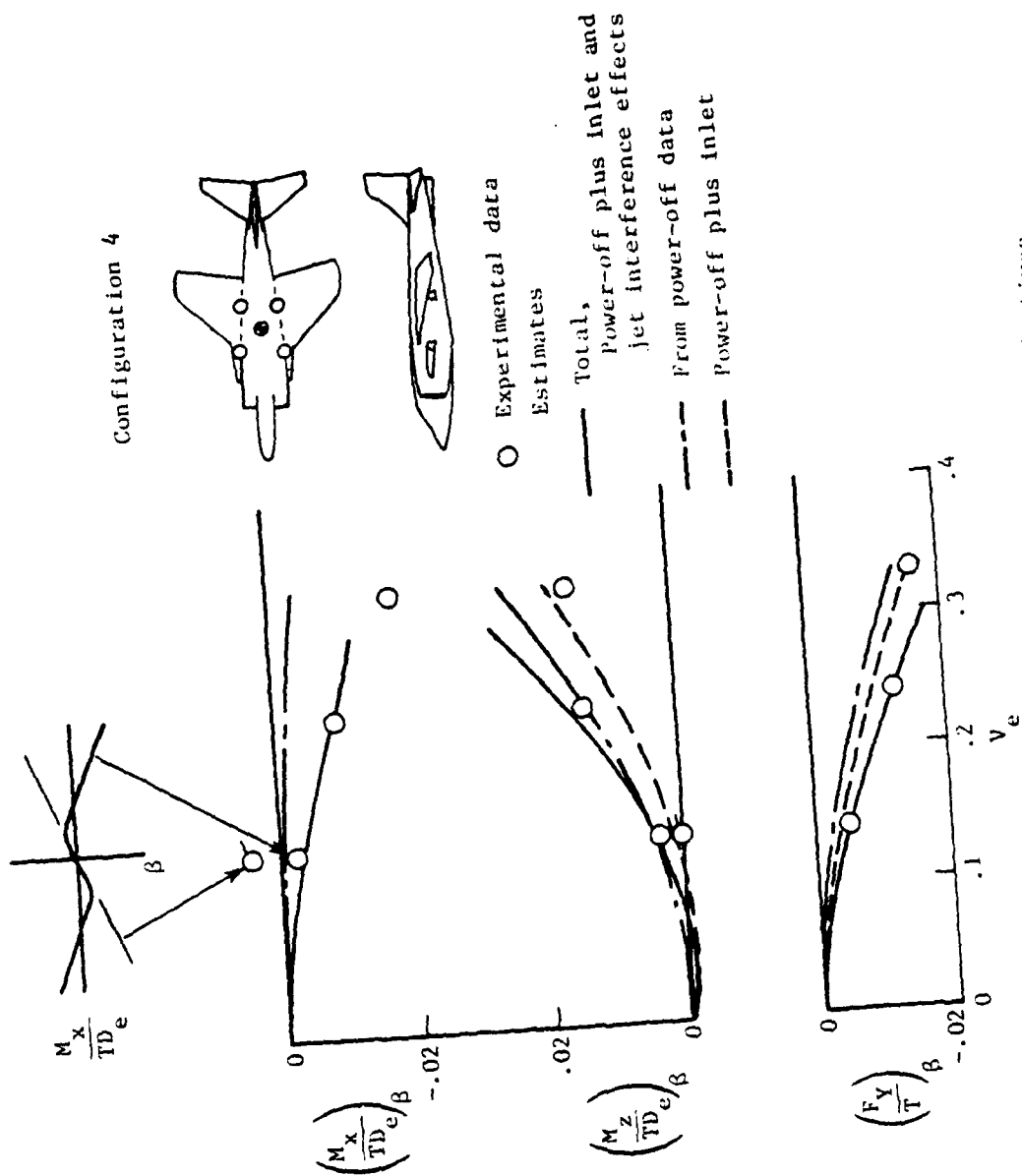


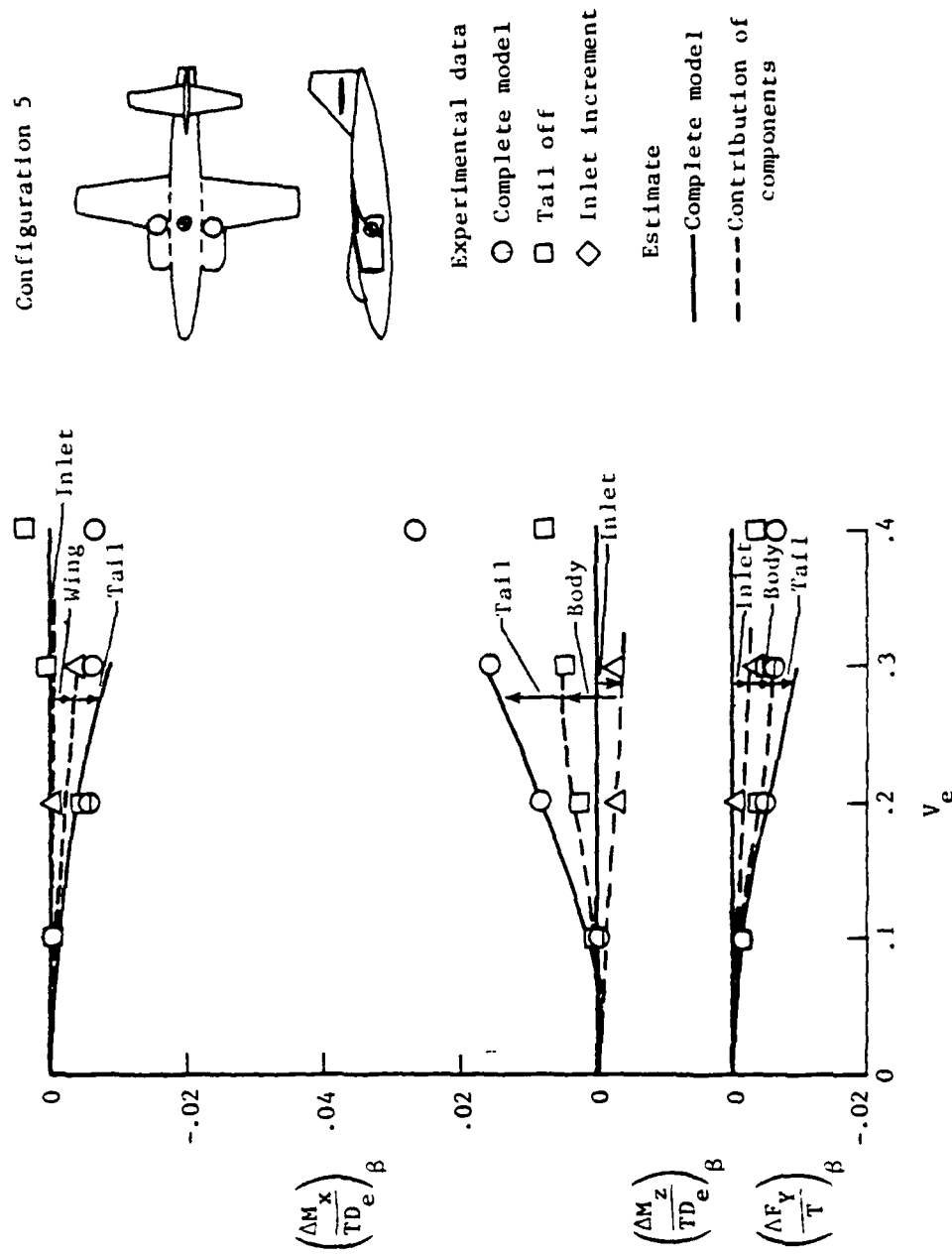
Figure 10.- Comparison of estimate with data for configuration 4 (ref. 7).

(Configuration 17 of ref. 1) $\left(\frac{\dot{w}_1}{\dot{w}_j} = .5\right)$



(b) Total lateral directional derivatives.

Figure 10.- Concluded.



(a) Induced increments.

Figure 11.- Comparison of estimate with data for configuration 5

(ref. 5) (Configuration 11a of ref. 1) $\left(\frac{\dot{w}_1}{w_j} = .5 \right)$.

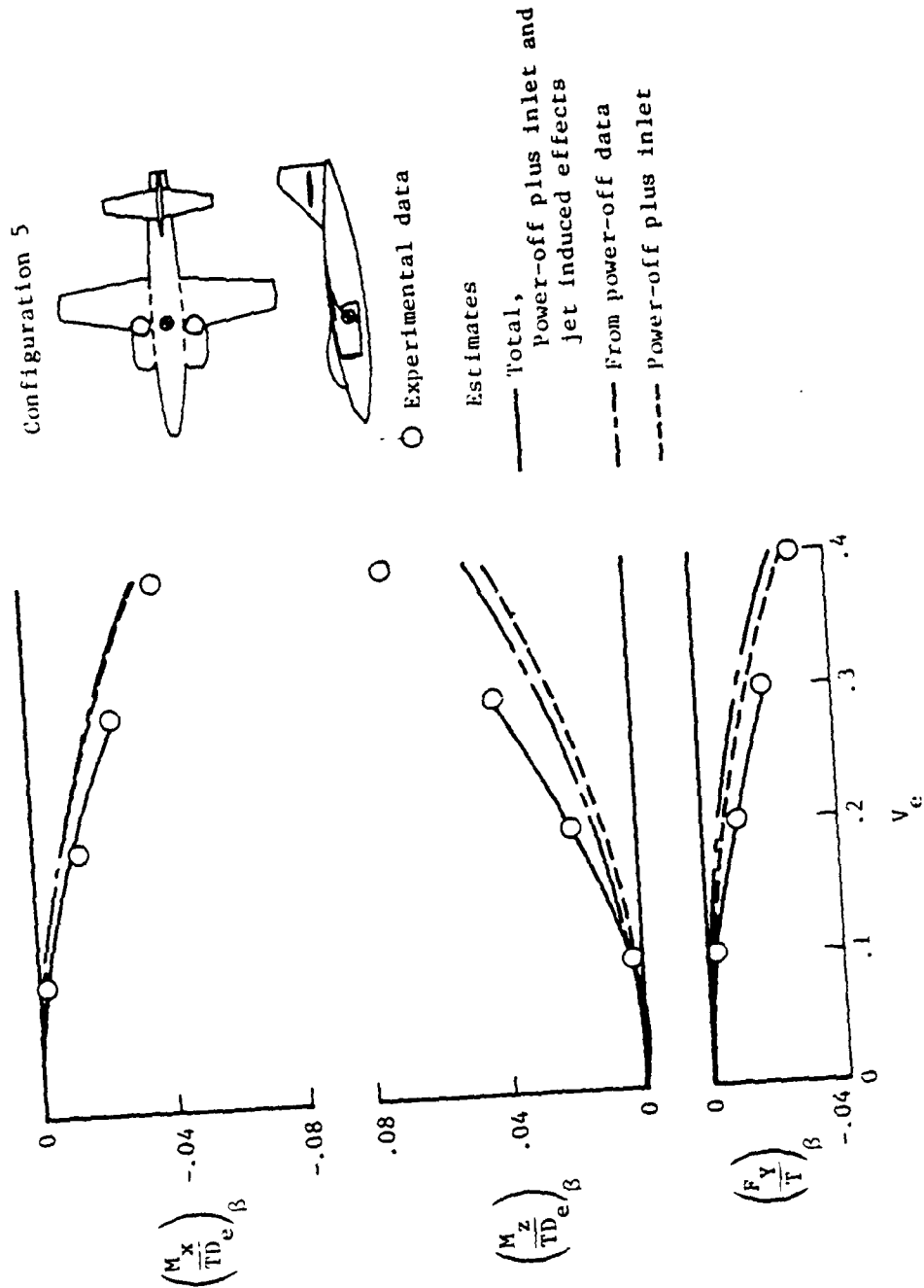
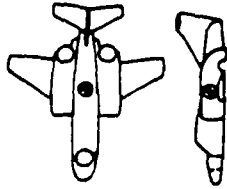
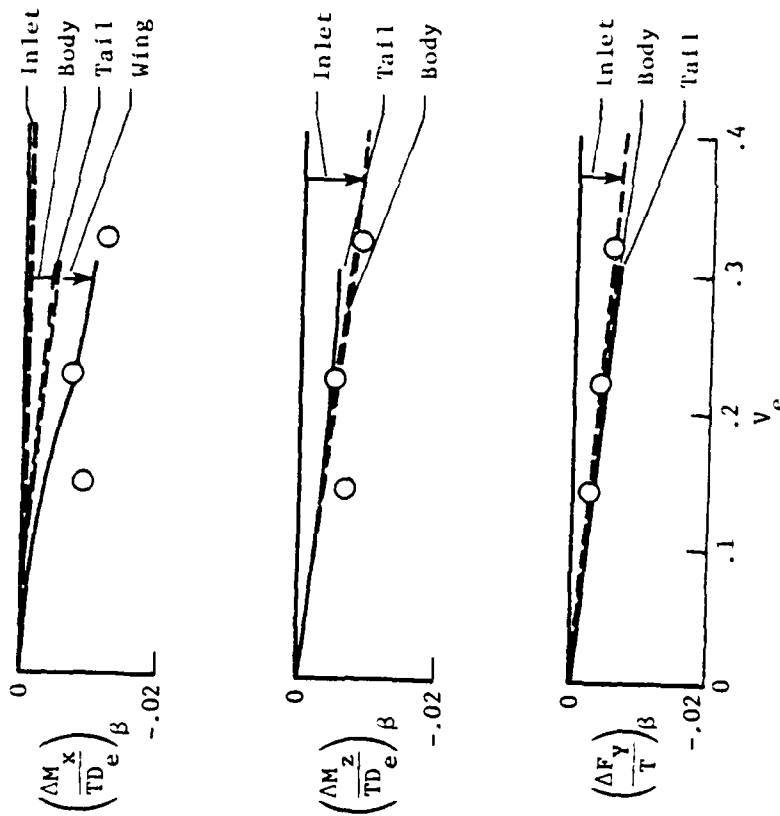


Figure 11.- Concluded.

Configuration 6



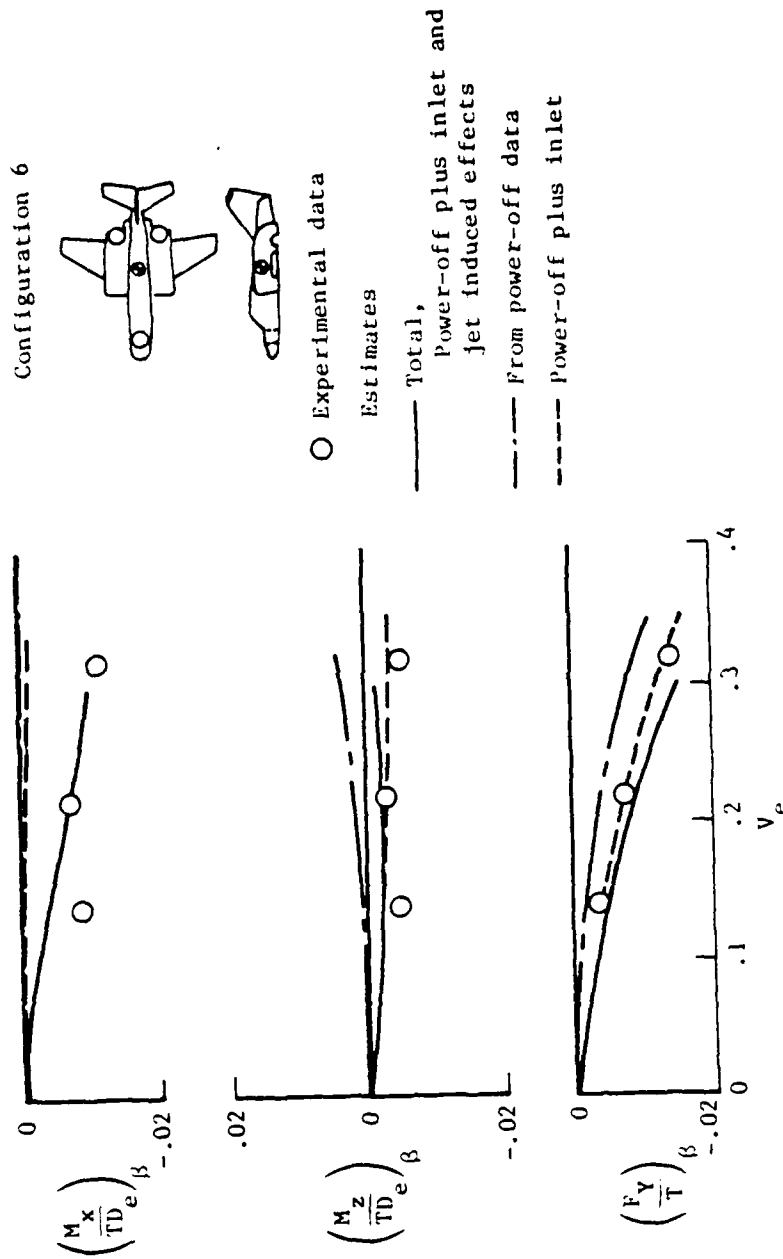
○ Experimental Data
 — Complete model Estimate
 - - - Contribution of components



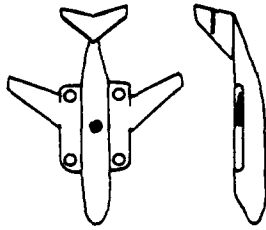
(a) Induced increments.

Figure 12.- Comparison of estimate with data for configuration 6 (ref. 10).

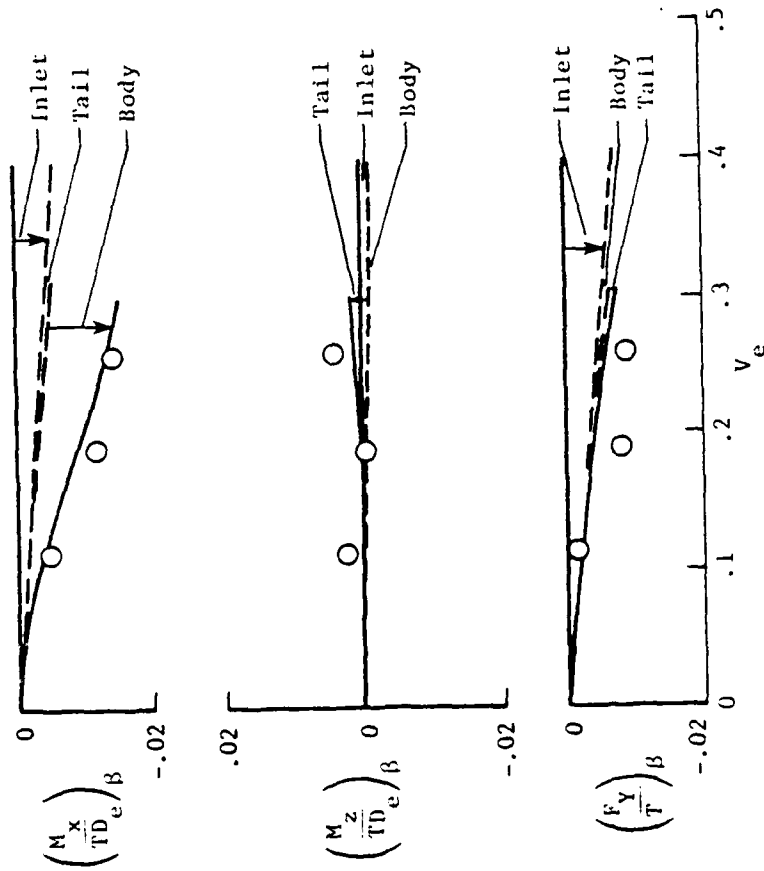
(Configuration 14 of ref. 1) $\left(\frac{\dot{w}_i}{\dot{w}_j} = 1.0 \right)$



Configuration 7



○ Experimental data
 Estimate
 — Complete model
 - - - Contribution of components



(a) Induced increments.

Figure 13.- Comparison of estimate with data for configuration 7 (ref. 11).

$$\left(\frac{\dot{w}_i}{\dot{w}_j} = 1.0\right)$$

(Configuration 13 of ref. 1)

Configuration 7

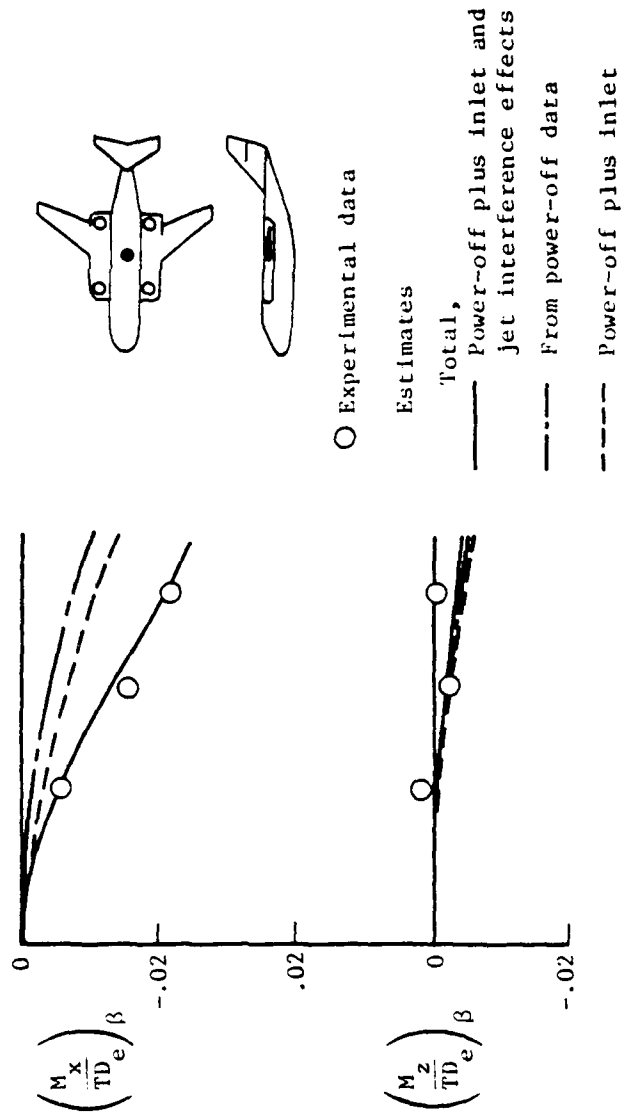
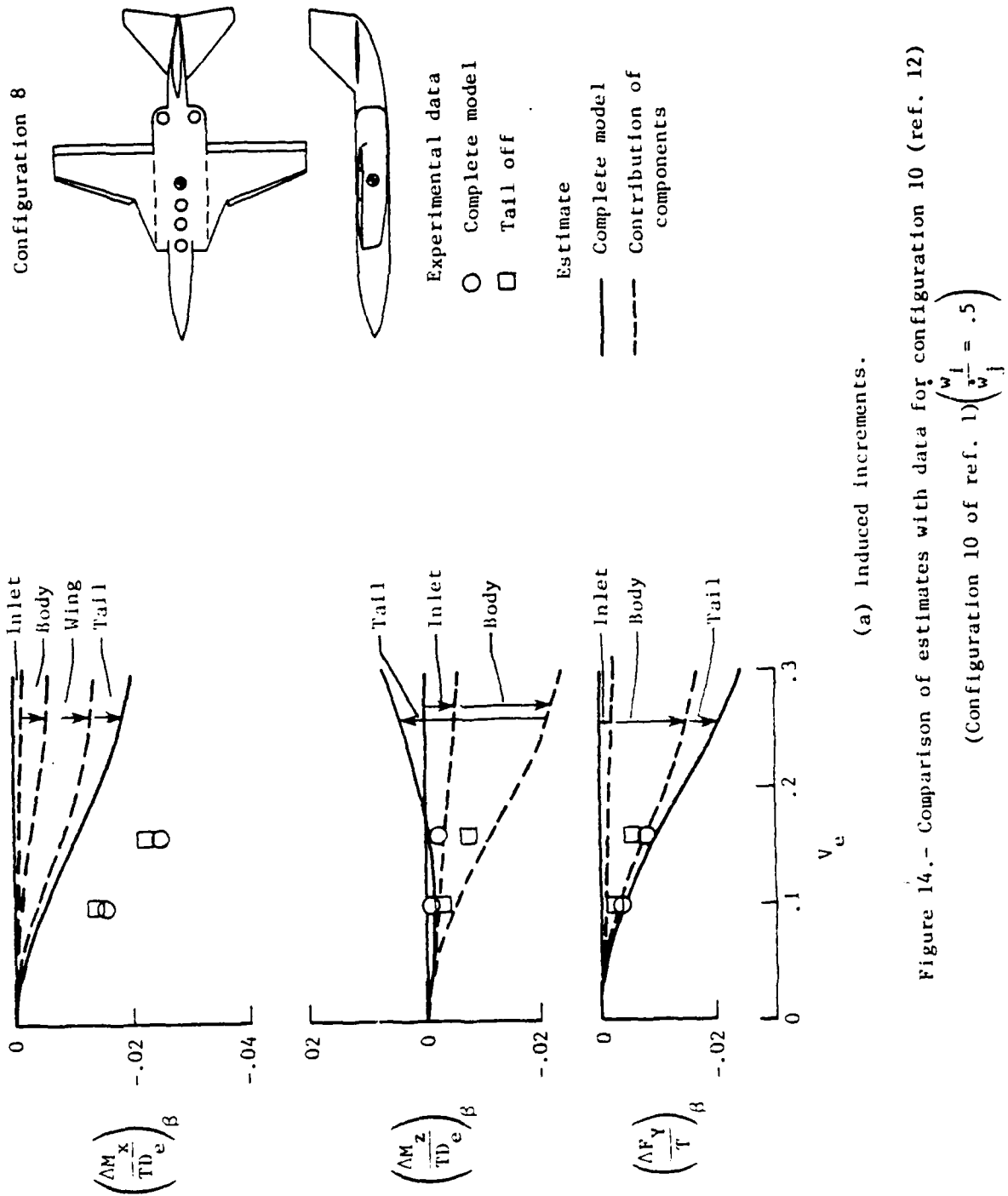
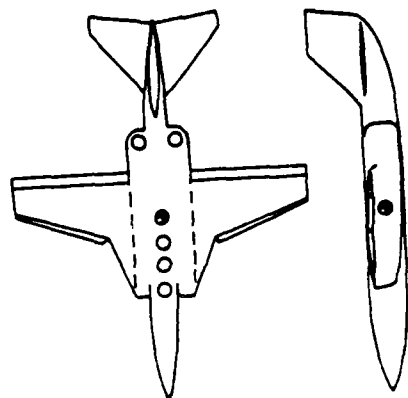


Figure 13.- Concluded.



Configuration 8



○ Experimental data

Estimates

— Total, power off plus inlet and jet induced effects

- - - From power-off data

- - - Power-off plus inlet

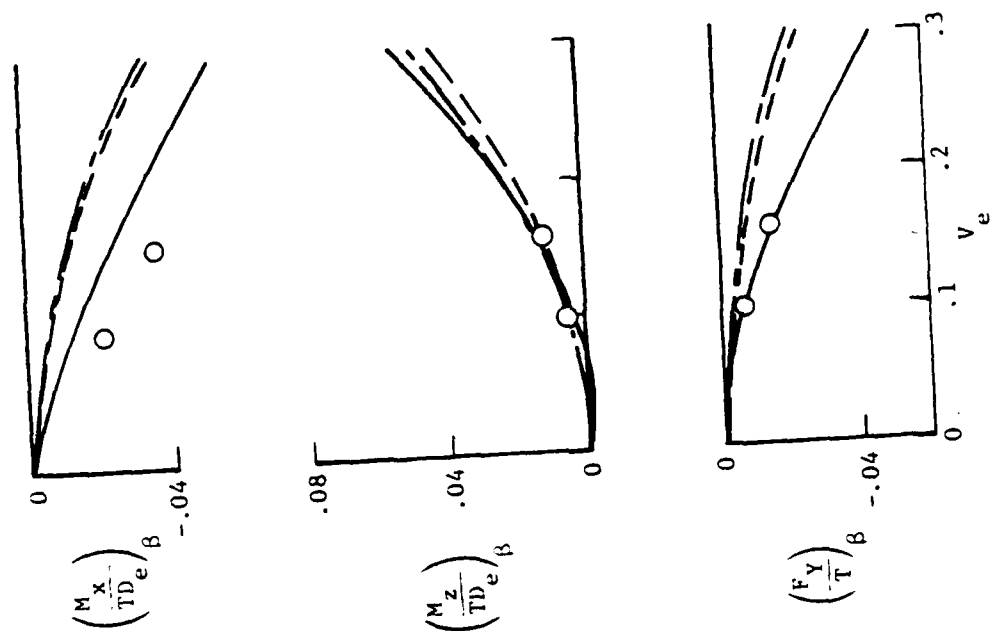


Figure 14.- Concluded.

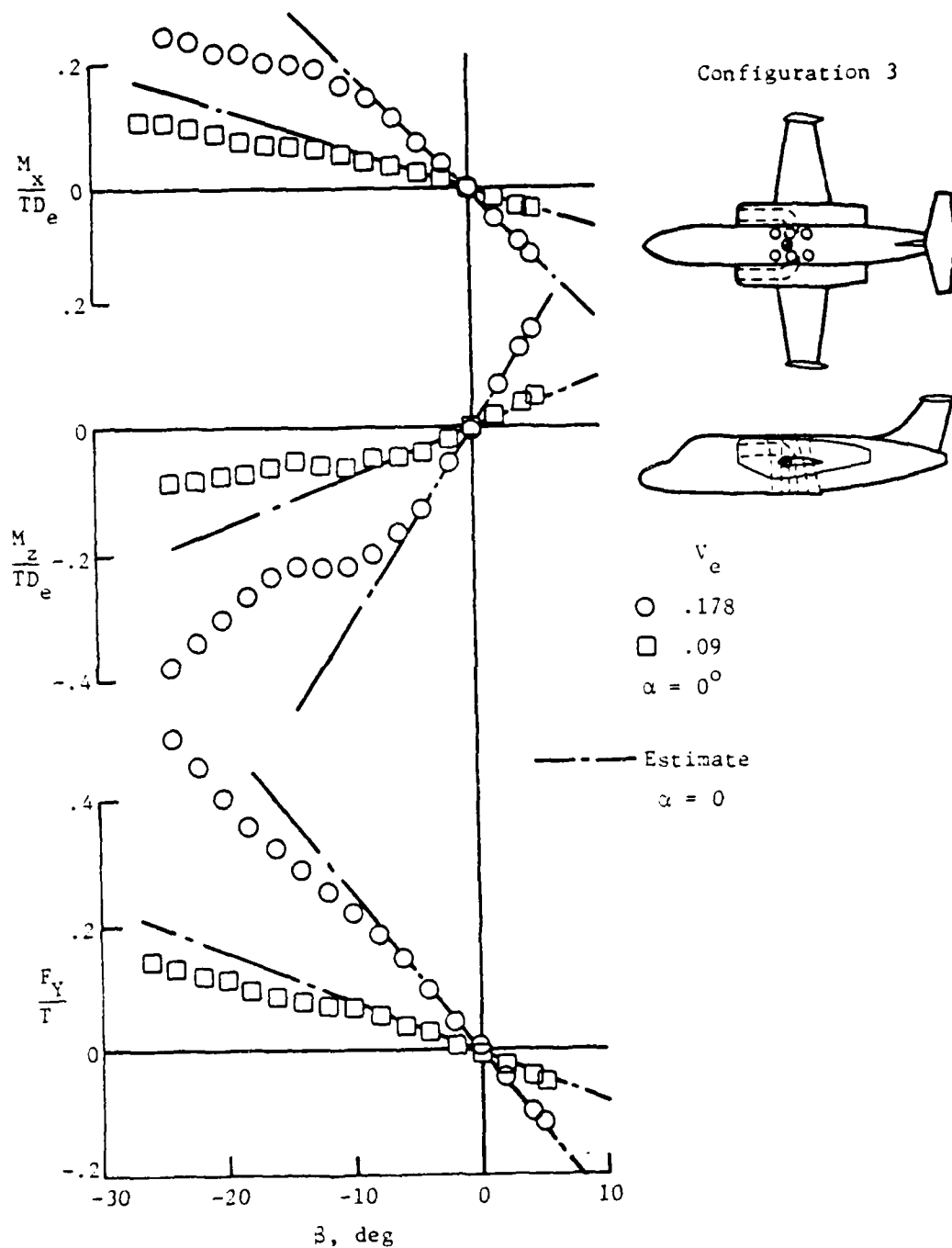
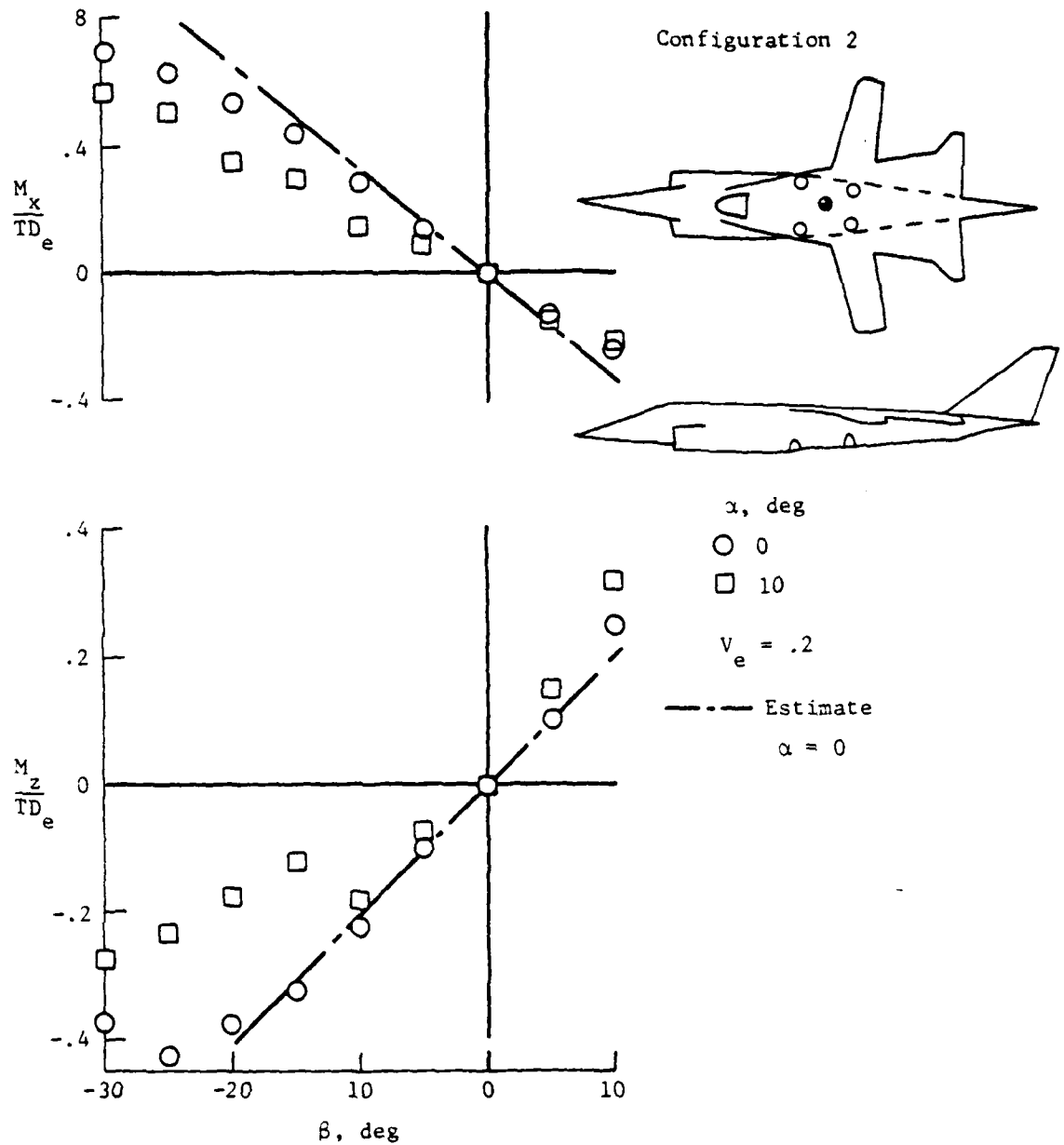
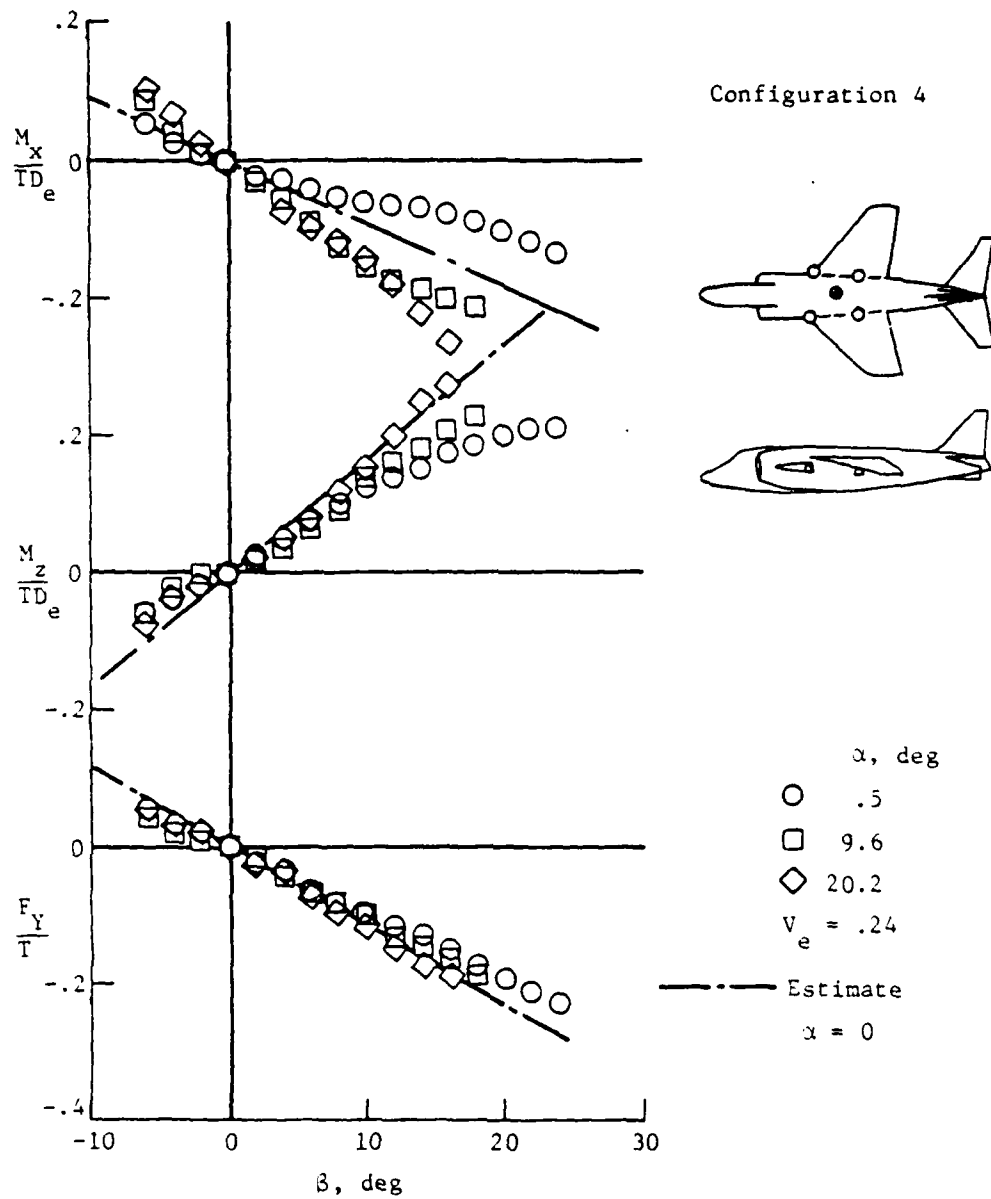


Figure 15.- Effect of large angles of sideslip.
Configuration 3 at zero angle-of-attack.

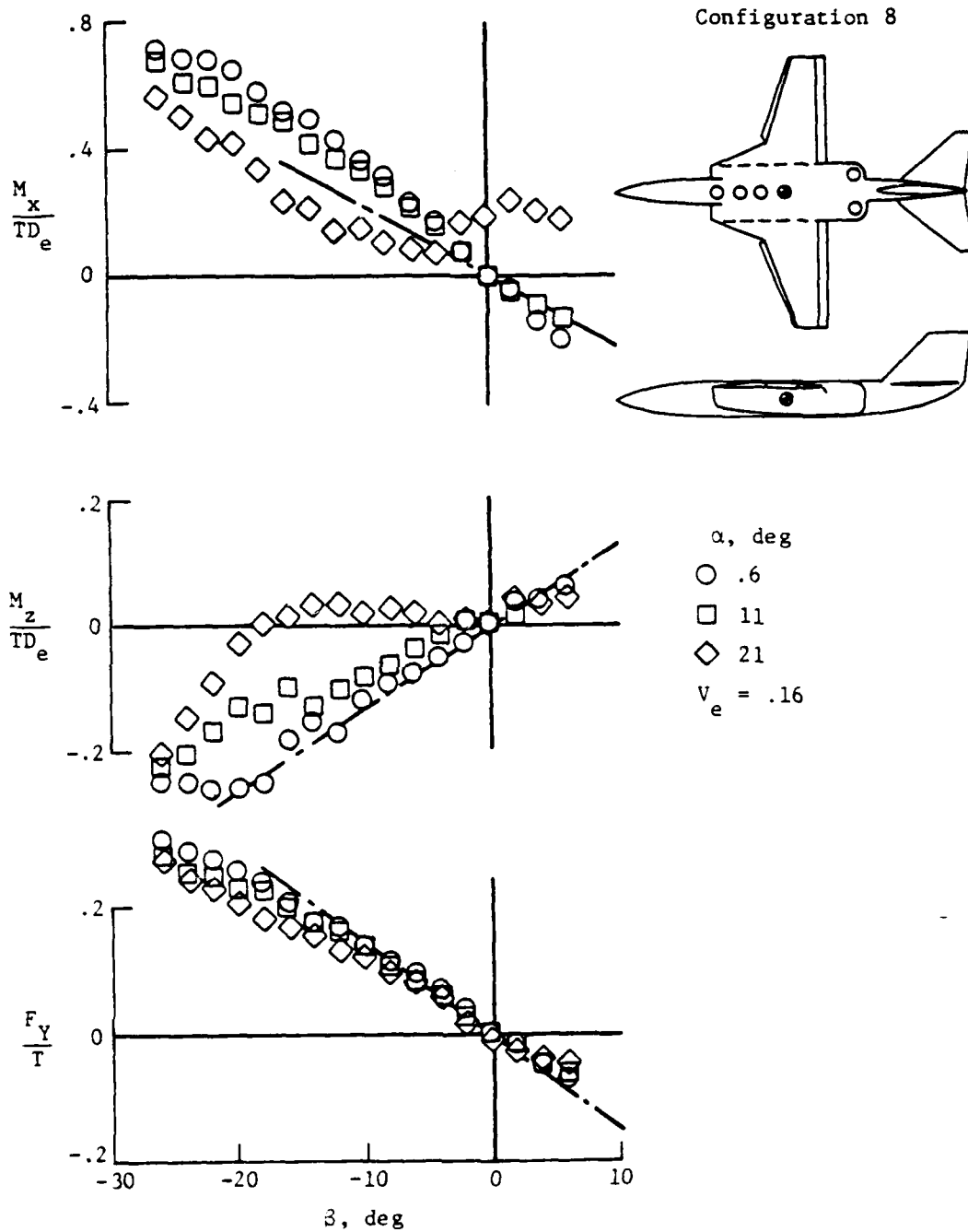


(a) Configuration 2.

Figure 16.- Effect of large combined angles.



(b) Configuration 4.
Figure 16.- Continued.



(c) Configuration 8.

Figure 16.- Concluded.

D I S T R I B U T I O N L I S T

REPORT NO. NADC-81Q31-60

AIRTASK NO. A03V-320D/01B/7F41-400-000

No. of Copies

NAVAIR (AIR-950D)	4
(2 for retention)	
(1 for AIR-320D)	
(1 for AIR-5301)	
NAVWPNCEN, China Lake, CA	1
NAVAIRPROPCEN, Trenton, NJ.	1
DTNSRDC, Bethesda, MD (Attn: Dr. H. Chaplin)	1
ONR, Arlington, VA (Attn: R. Whitehead).	1
NAVPGSCOL, Monterey, CA (Attn: M. Platzer)	1
NASA, Ames Research Center, Moffett Field, CA	2
(1 for D. Hickey)	
(1 for W. Deckert)	
NASA, Langley Research Center, Hampton, VA (Attn: R. Margason)	1
NASA, Lewis Research Center, Cleveland, OH.	1
Wright-Patterson AFB, Dayton, OH.	2
(1 for Flight Dynamics Lab)	
(1 for Aeronautical Systems Division)	
The Pentagon, Washington, DC (Attn: R. Siewert)	1
U.S. Army Aviation Systems Command, St. Louis, MO	1
U.S. Army Research Office, Durham, NC	1
DTIC, Alexandria, VA.	12
Boeing Company, Seattle, WA (Attn: E. Omar).	1
LTV Aerospace Corporation, Dallas, TX	2
(1 for T. Beatty)	
(1 for W. Simpkin)	
Rockwell International, Columbus, OH (Attn: W. Palmer)	1
General Dynamics Corporation, Ft. Worth, TX (Attn: W. Folley).	1
Nielson Engineering, Mountain View, CA (Attn: S. Spangler)	1
Univ. of Tennessee, Space Inst., Tullahoma, TN (Attn: W. Jacobs)	1
Lockheed-California Co., Burbank, CA (Attn: Y. Chin)	1
Northrop Corporation, Hawthorne, CA (Attn: P. Wooler).	1
Grumman Aerospace Corp., Bethpage, LI, NY (Attn: S. Kalamaris).	1
Royal Aeronautical Establishment, Bedford, England (Attn: A. Woodfield).	1
Fairchild-Republic, Corporation, Farmingdale, LI, NY.	1
Calspan, Buffalo, NY.	1
McDonnell Douglas Corp., St. Louis, MO (Attn: Dr. D. Kotansky)	1
V/STOL Consultant, Newport News, VA (Attn: R. Kuhn).	1
Georgia Inst., of Technology, Atlanta, GA (Attn: Dr. H. McMahon)	1
Penn State Univ., Univ. Park, PA (Attn: Prof. B. W. McCormick)	1